THE PENNSYLVANIA STATE UNIVERSITY
SCHREYER HONORS COLLEGE

DEPARTMENT OF ELECTRICAL ENGINEERING

SIMULATING THE MECHENICAL AND ELECTRICAL PROPERTIES OF A DESIGNED MAGNETOELECTRIC RESONANT GATE TRANSISTOR

YUFEI WU
Spring 2012

A thesis
submitted in partial fulfillment
of the requirements
for a baccalaureate degree
in Electrical Engineering
with honors in Electrical Engineering

Reviewed and approved* by the following:

Suman Datta
Professor of Electrical Engineering
Thesis Supervisor

Julio Urbina
Assistant Professor of Electrical Engineering
Honors Adviser

* Signatures are on file in the Schreyer Honors College.

Abstract

The resonant gate transistor concept was first brought up by Nathanson et al. in 1967 for sensing displacement. This great work has opened the door for mechanical movement sensing with field effect transistor as read-out component. Inspired by the amplification of transistor and the transduction among electrical, magnetic, and mechanical energy domain realized by cantilever resonance, a magnetoelectric resonant gate transistor (MERGT) has been designed and fabricated, demonstrating a nanoTesla magnetic field detection sensitivity at room temperature.

This thesis presents numerical simulations of the mechanical properties of the resonant gate and the electrical properties of the n-channel field effect transistor with two commercially available software packages, COMSOL Multiphysics and TCAD Sentaurus respectively. The frequency response of the resonating cantilever is studied and the effects of residual stress due to thermal processes during fabrication and air damping in cantilever oscillation are analyzed. For the electrical part, the Id-Vg characteristics of the nFET are simulated. Also, the amplification of small ac signal is demonstrated. After considering the laws governing cantilever vibrations, flux concentration effect in a magnetic field, and cantilever stiffness variations, an analysis is conducted to propose an improved resonant gate dimensions aiming at achieving higher gate sensitivity. Lastly, the numerical simulation results are compared with the experimental measurements and possible improvements of the designed MERGT in the future are discussed.

Table of Contents

List of Figures

List of Tables

Acknowledgement

I would like to thank my honors thesis advisor Dr. Suman Datta for his patience and support. I cannot imagine myself to be at where I am today without his help. Also, I would like to thank graduate student Feng Li who provided all the experimental data and generously helped me whenever I have troubles alone my way of research. I would also like to thank Dr. Julio Urbina, my honors advisor, who has been guiding me and giving me advices ever since I entered the Schreyer Honors College. Lastly, I would like to thank my family for always supporting me and believing in me.

Chapter 1

Introduction

1.1 A Brief Introduction to MEMS

MEMS is short for Microelectromechanical Systems and is a field evolved from the integrated circuit industry. The development of the MEMS is to a large extent driven by the advancing of IC-based micromachining technology. In 1959, before the formation of the name “MEMS”, the famous physicist Richard Feynman gave the lecture titled “There is plenty of room at the bottom” at an American Physical Society meeting. In the lecture, Feynman described the enormous amount of space available on the microscale. That lecture foreshadowed the rapid development of micromachining and in turn MEMS in the near future [1]. After that year, in 1964, the first engineered batch-fabricated MEMS device, which is a resonant gate transistor, was demonstrated by Natheson et al. The invention brought the unconventional concept of resonant gate to the world and turned out to have a huge influence on the development of microsensors following that. In the 1970s, Kurt Petersen at the IBM research laboratory, along with other colleagues, developed diaphragm-type silicon micromachined pressure sensors. Very thin silicon diaphragms with embedded piezoresistive sensors were made using silicon bulk micromachining. The diaphragm deforms under differential pressures, including mechanical stress that was picked up by the piezoresistors. This fact makes the diaphragm more sensitive than conventional membrane-type pressure sensors [2]. Besides the noticeable inventions described above, there are many other great innovative accomplishments which all contribute to the fast development of MEMS ever since its existence. Nowadays, after MEMS has been under research for so many years, the entire field has formed systematic structures which divide the MEMS into different application branches. The table below shows the representative major branches of MEMS Technology.

Area of Research	Perceived drivers of technology
Optical MEMS	Monolithic integration of mechanics, electronics, and optics Unique spatial or wavelength tunability Improved efficiency of optical assembly and alignment accuracy
BioMEMS	Miniaturization (minimal invasion and size matched with biological entities) Rich functional integration within physically small, minimally invasive medical devices
Microfluidics(laboratory-on-a-chip or micro total analysis systems	Reduced amount of samples and reagents and associated cost Parallel and combinatorial analysis possible Miniaturization, automation, and portability

Radio Frequency (RF) MEMS	Unique performances not found in solid-state RF integrated devices Promises of direct integration of active and passive elements with circuitry
Nano Electromechanical Systems (NEMS)	Unique physical properties due to scaling (e.g., ultra-low mass and ultra-high resonant frequency) Unprecedented sensitivity and selectivity of detection achievable in selected cases

Table 1.1 Representative major branches of MEMS technology. Taken from [2]

It is noticeable that MEMS technology is so encompassing in our daily lives now but at the same time, many people have not really realized it. For example, one of the great functions of iPhone as well as that of many smart phones today cannot be realized without the assistance of MEMS technologies. The rotation of webpages and pictures to match the orientation of an iPhone is realized by a microaccelerometer embedded inside the phone [3]. It is not hard to tell that MEMS will keep playing a more and more important role in our lives in the near future.

1.2 Intrinsic Characteristics of MEMS

From the name "Microelectromechanical", we can immediately see that one of the distinct features of MEMS is small size. As we dig into the field, we will start to understand that there are more attractive features MEMS can provide than just small size. To be concise, the most generic and distinct merits of MEMS can be generalized as three Ms. That is, miniaturization, microelectronics integration, and mass fabrication with precision [4].

Miniaturization

As indicated by the prefix "Micro", the typical length scale of MEMS devices ranges from 1 μm to 1 cm. By shrinking the device sized down to this level, many properties of the devices will change accordingly. Thus, we must be extremely careful when scaling the device sized down. Small dimensions can offer many operational advantages, such as soft springs and high resonance frequency. However, miniaturization can also bring about disadvantages. Some physical phenomena do not scale favorably when the dimensions are reduced while other physical phenomena that work poorly at the macroscale become very practical and attractive at the microscale. To clarify on this, two examples are demonstrated below.

The stiffness of a cantilever is defined by its spring constant. The formula governing the spring constant is

$$k = \frac{Ewt^3}{4l^3}$$

where E is Young's modulus of elasticity, w, t, and l are cantilever width, thickness, and length respectively. Assume

$$w = \alpha l$$
$$t = \beta l$$

then the spring constant can be expressed as

$$k = \frac{Ewt^3}{4l^3} = \frac{E\alpha\beta^3 l^4}{4l^3} = \frac{E\alpha\beta^3}{4} l$$

This indicates that the smaller the dimension of the cantilever, the softer the cantilever is. And softer cantilever further indicates higher achievable resonance frequency.

Another example can show us how the area-to-volume ratio of a 3D object changes as we scale down the object's size.
Assume we have a cube with L as the length of each edge. Then the area-to-volume ratio can be represented as

$$\frac{area}{volume} = \frac{6L^2}{L^3} = 6\frac{1}{L}$$

We can see that the area-to-volume ratio increases as we reduce the size of the object. This conclusion is applicable to any arbitrary shaped 3D objects too. Surface forces (such as van der Waals force, friction, and surface tension), which depend on object areas, are important for the behavior of microscale objects. Volume forces (such as gravitational force), which depend on object volumes, are important for the behavior of macroscale objects.

Microelectroincs Integration

One attractive feature of MEMS is the ability to integrate mechanical sensors and actuators with electronic processors and controllers at the chip level. This process paradigm is referred to as monolithic integration-fabrication of various components on a single substrate in an unbroken, wafer-level process flow [2]. Monolithic integration makes it possible to realize large and dense array of sensors and actuators. It also helps to manufacture many portable mechanical devices. However, there always exists the problem of balance between pros and cons. The benefits of monolithic integration should be weighed against other concerns, such as cost and time.

Mass Fabrication with Precision

As mentioned in previous section, the development of MEMS is based on the advance of IC-based micromachining technology. Mass fabrication is realized by the standard semiconductor fabrication procedures. Modern lithography technology can achieve high precisions and makes MEMS practical.

1.3 Sensors and Their Design Criteria

MEMS sensors have experienced great success in both physical sensing contexts and chemical/biological sensing contexts ever since the publication of a paper by Smith about certain stress sensitive effects in silicon and germanium termed piezoresistance [5]. Physical sensors measure physical variables such as force, acceleration, temperature, magnetic field strength, and acoustic vibration. Chemical/Biological sensors detect variables such as chemical concentration, pH, DNA sequence, molecular binding strength. Among all these, piezoelectric effect has been widely used as a mechanism to measure magnetic field strength by converting magnetic signal to mechanical motion through bending of cantilevers. The designed Magnetoelectrice Resonant Gate Transistor to be studied in this thesis also falls into the category of MEMS sensors. It was designed to detect tiny magnetic signal through transduction of magnetic energy to mechanical energy realized by a cantilever and through further signal amplification using an n-channel field-effect-transistor. Unlike the usually preferred piezoelectric effect in magnetic field sensing, magnetostrictive effect is used in our sensor instead. Same as other macroscale sensors, MEMS sensors are subject to some design criteria and in the following text, I will be discussing some of the most important design characteristics.

Sensitivity

Sensitivity is defined as the ratio between the magnitude of the output signal and that of the input stimulus. This is one of the most important evaluation criteria of a sensor since the basic task for a sensor is to detect. Sensitivity of a sensor can depend on many things such as the magnitude and frequency of input signals, environment, biasing level.

Responsivity

Responsivity is also known as the accuracy, resolution, or detection limit. It is generally limited by the noise associated with the transduction elements and circuits. Interference noise, such as the presence of the earth magnetic field when measuring a small magnetic signal, can be reduced and eliminated by careful shielding setup. Random noises, on the other hand, have more fundamental origins and usually can limit the responsivity of a designed sensor. For MEMS sensor applications, the responsivity is limited by two major noise mechanisms: Johnson noise and the 1/f noise [6].

Johnson noise is white noise and is due to random thermal fluctuation of internal electrons and particles [2]. The 1/f noise, also known as flicker noise or pink noise, is the result of conductance fluctuation when a current passes through a resistor [2].

Signal-to-noise ratio (SNR)

The SNR is the ratio between the magnitude of signals and noise.

There are many other design criteria to be taken into account such as bandwidth, sensor reliability, cross talk or interference, and development cost and time. For the purpose of this thesis, I will mainly focused on the above three discussed characteristics.

1.4 Micromachining

The fabrication process for MEMS devices is called micromachining. Many of the microfabrication techniques and materials used to produce MEMS devices have been borrowed from the IC industry. In fact, MEMS devices were first developed on silicon wafers because of the easy availability of mature processing technologies that had been developed within the microelectronics industry [2]. The two most fundamental classes of fabrication technologies are bulk micromachining and surface micromachining. As suggested by the names, bulk micromachining involves selectively etching inside the bulk materials while surface micromachining involves succession of thin films deposition and selective etching.

Bulk micromachining is an important class of the MEMS process and is the most widely used technique for silicon sensor fabrication. Bulk micromachining can be applied to silicon, glass, gallium, arsenide, and other materials of interest. One great example of a device made using the bulk micromachining method is the earliest micromachined pressure sensor where two wafers are involved: a bottom wafer is etched to form a cavity and a top wafer is used to make the membrane [7].

The second class of microfabrication processes for MEMS is surface micromachining. One typical technique widely used for fabricating dynamic MEMS devices is the selective removal of an underlying layer, or sacrificial layer. Figure 1.1 below illustrates a surface micromachining process.

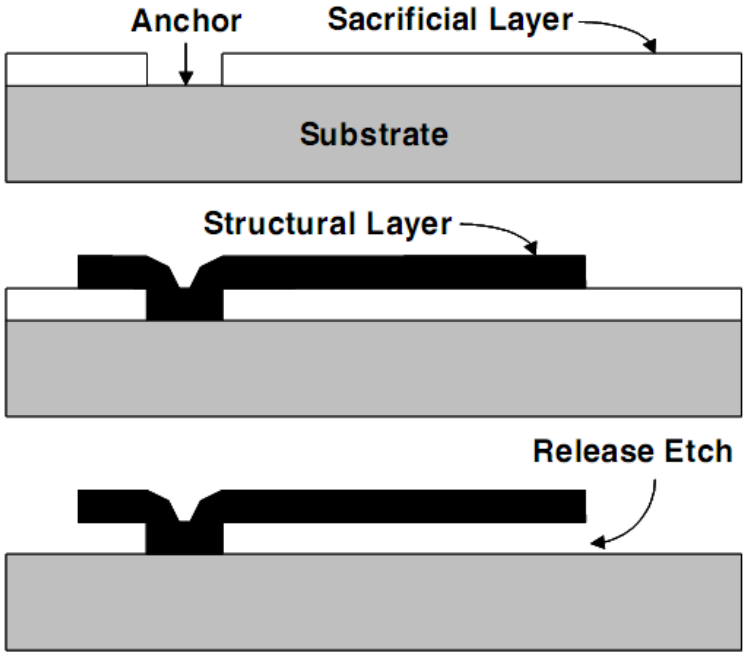

Figure 1.1 Surface micromachining and the sacrificial layer technique. Taken from [1].

As show in the picture, a sacrificial layer is first deposited and patterned on a substrate. Then a structural layer is deposited on top of the sacrificial layer. Following these two steps, the sacrificial layer is selectively removed to free the structure layer on top. The cantilever resonant gate in our sensor was fabricated using this technique.

Chapter 2

CANTILEVER GATE OF A DESIGNED MAGNETOELECTRIC RESONANT GATE TRANSISTOR

2.1 Cantilever Structure and Common Properties

A beam is a structure member subjected to lateral loads, i.e., forces or moments having their vectors perpendicular to the longitudinal axis. The types of beams encountered most frequently in MEMS are fixed-free (cantilever) and fixed-fixed (bridge) beams. Below is a table showing the two different structures.

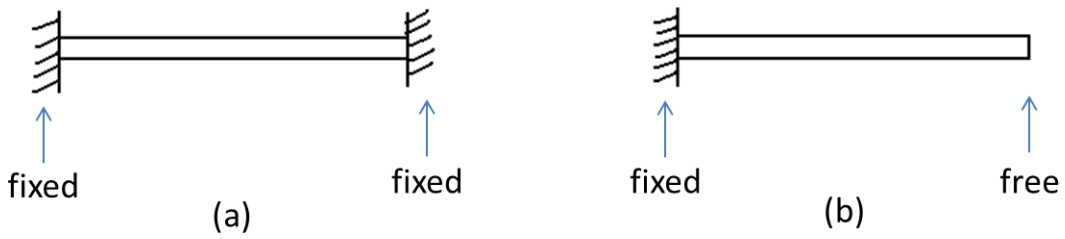

Figure 2.1.1 (a) A fixed-fixed beam and (b) A fixed-free beam.

For the magnetoelectric resonant gate transistor (MERGT) studied in this thesis, the resonant gate is a three-layer fixed-free cantilever where the free end serves to modify the channel charge density of the underlying n-channel field-effect-transistor through a vibration induced air-gap capacitance modulation. The oscillation of the cantilever is induced by the magnetostriction of the middle layer which is a magnetostrictive material (Metglas) under a DC magnetic field modulated by a small AC magnetic signal. The overall effect of the MERGT is to convert an input magnetic signal to an output current signal that can be read by some nowadays commercially available measuring devices. It can be used in biomedical imaging applications and even challenge the SQUIDS for brain signal detection. Before getting into the software simulation, I will first briefly talk about some of the equations dominating the mechanical properties of a moving cantilever such as spring constant, resonance frequency, and deflection of a cantilever.

2.1.1 Stress and Strain

There are two types of mechanical stresses, normal stress and shear stress. Consider a simple cube with a uniform cross-sectional area subjected to axial loading. If we pull on the rod in its longitudinal direction, it will experience tension and the length of the cube will increase. Imaging a cut through the cube at a section, a continuously distributed force will be acting over the entire

area of the section. The intensity of this force is called the stress and if the stress acts in a direction perpendicular to the cross section, it is called normal stress. The normal stress, commonly denoted as σ , is defined as

$$\sigma = \frac{F}{A}$$

Here F is the force and A is the cross-sectional area. Strain is the unit elongation of the cube and is defined as

$$\varepsilon = \frac{L - L_0}{L} = \frac{\Delta L}{L_0}$$

Shear stress, on the other hand, can be generated under different force-loading condition. One simple way is to apply a pair of force on opposite faces of a cube. The magnitude of the shear stress is defined as

$$\tau = \frac{F}{A}$$

And the shear strain represents the extent of rotational displacement. It is defined as

$$\gamma = \frac{\Delta X}{L}$$

Stress and strain are closely related according to Hooke's law:

$$\sigma = E\varepsilon$$

where E is called the modulus of elasticity or Young's modulus.

2.1.2 Mechanical Properties of Beams

The equation governing a beam deflection under a simple load condition is

$$EI\frac{d^2y}{dx^2} = M(x)$$

where $M(x)$ represents the bending moment at the cross section at location x , and y represents the displacement at location x . The x-axis runs along the longitudinal direction of the cantilever. For the most commonly encountered cantilever where the cross section is a rectangle with w , t as the width and thickness respectively, the moment of inertial with respect to the neutral axis is $I = \frac{wt^3}{12}$. The spring constant of cantilever with the same geometry obeys Hook's law and can be represented as $k = \frac{F}{x} = \frac{3EI}{l^3} = \frac{Ewt^3}{4l^3}$. Another property that is very important for MEMS devices is the intrinsic stress. It is often due to temperature difference during deposition and use since different materials have different thermal expansion coefficients. A common scenario of intrinsic stress induced beam bending involves a structure with two or more layers. Consider a cantilever consisting of two layers as shown in Figure 2.1.2.

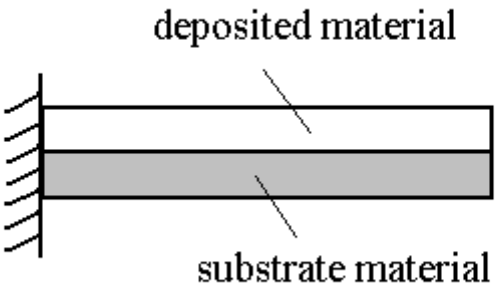

Figure 2.1.2 A cantilever consists of two layers

Assume the intrinsic stress in the substrate material to be zero, if the deposited layer has a tensile stress, the beam would bend upward (Figure 2.1.3 (a)) and if the deposited layer has a compressive stress, the beam would bend downward (Figure 2.1.3 (b)).

Figure 2.1.3 (a) Cantilever bending upward due to tensile residual stress

Figure 2.1.3 (b) Cantilever bending downward due to compressive residual stress

2.2 COMSOL Multiphysics Model

2.2.1 3-D Structure Construction

The first part of the designed MERGT to be studied here is the three-layer cantilever resonant gate with Titanium (Ti), Metglas, and Platinum (Pt) used as the materials for the bottom, middle, and top layers respectively. COMSOL Multiphysics 3.5a, which is a finite element analysis simulator, is chosen as the software package used to simulate the motion of the gate under the existence of an external force. Since COMSOL Multiphysics does not have a built-in module for magnetoelectric sensors, I decoupled the magnetoelectric effect into magnetostriction and mechanical vibration of the cantilever gate. Under this assumption, I simulated the mechanical movement of the gate in COMSOL Multiphysics after taking the response of the magnetostrictive layer to an applied ac magnetic signal as an input. In this way, the problem now has been refined to a simulation of the deflection frequency response of the Ti-Metglas-Pt three-layer cantilever with respect to an input force.

After launching COMSOL Multiphysics 3.5a, the first step is to choose the space dimension and application module to be used in the model navigator panel. I chose 3D under the space dimension tab and Solid, Stress-Strain Frequency response analysis under the Structural Mechanics tap belonging to the MEMS Module [8].
In the drawing interface following the model navigator panel, I set up work-plane, drew geometries in 2D, and then extruded for every layer separately. The dimensions of the three-layer cantilever simulated are shown in the table below.

	Titanium	Metglas	Platinum
Length (um)	3	3	3
Width (um)	1	1	1
Thickness (nm)	500	100	50
Position	Bottom	Middle	Top

Table 2.2.1 Dimensions of the cantilever gate model in COMSOL Multiphysics.

The actual fabricated gate dimensions are shown in table 2.2.2.

	Titanium	Metglas	Platinum
Length (um)	300	300	300
Width (um)	100	100	100
Thickness (nm)	500	100	50
Position	Bottom	Middle	Top

Table 2.2.2 Dimensions of the cantilever gate fabricated.

It can be noticed that the length and width of the gate simulated in COMSOL are scaled by 1/100

from the original fabricated gate dimensions. This is mainly due to the fact that defining a mesh condition fine enough and solving for the equations governing the gate resonance of a structure in COMSOL Multiphysics with exactly the same dimensions as the one fabricated will take a great amount of time and require a large computer RAM size. If I try to define a coarse mesh to reduce the time and RAM space needed for simulation, the results will not be accurate enough. Under this scenario, considering the fact that cantilever resonant frequency has a $\frac{1}{L^2}$ dependence on its length, an alternative way is to use the above describe dimensions in simulation and modify the results according to the $\frac{1}{L^2}$ dependence of frequency.

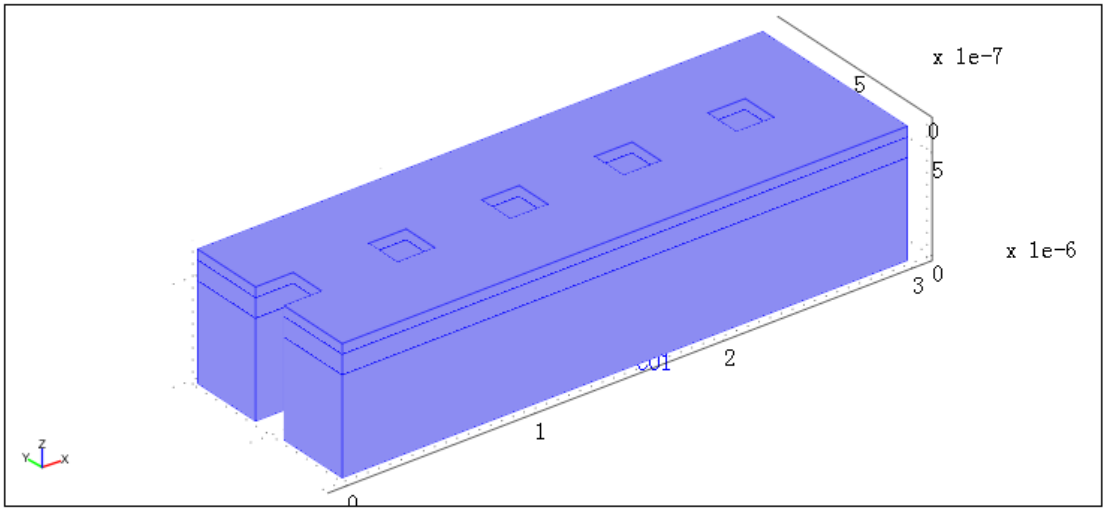

Figure 2.2.1 Cantilever gate structure simulated in COMSOL Multiphysics.

One thing to clarify about the structure shown above is the five cube-shaped cavities existing in the central region of the cantilever. These five cavities were etched away during the fabrication process after the completion of the three-layer gate structure. The reason for this extra step is to reduce influence of the friction due to surrounding air when the gate oscillates. In COMSOL Multiphysics, the "Difference" function was used to realize the cavity structure. The dimensions of the cavities are $20\mu m \times 20\mu m$ for the actual device and $0.2\mu m \times 0.2\mu m$ in simulation. And the space between two squares is $40\mu m$ and $0.4\mu m$ in reality and in simulation respectively.

2.2.2 Property Setups in COMSOL Multiphysics

After completing the build-up of the 3-D gate structure, the next step was to set up physics in the model. In this case, the major aspects to be considered were subdomain settings, boundary settings, and edge settings.

For subdomain settings, material properties including Young's modulus, Poisson's ratio, Thermal

expansion coefficient, and density need to be specified. Also, different mode of damping can be defined here for the subdomain of interest. Table 2.2.3 below presents the setup for each of the three domains of the cantilever.

	Subdomain 1	Subdomain 2	Subdomain 3
Material	Titanium	Metglas	Platinum
Young's modulus (Pa)	1.16E+11	1.1E+11	1.68E+11
Poisson's ratio	0.32	0.3	0.38
Thermal expansion coefficient (1/K)	8.60E-06	1.27E-05	8.80E-06
Density (kg/m^3)	4506	7700	21450

Table 2.2.3 Material Properties for each of the three layers of the cantilever.

For damping consideration, since the first simulation to be conducted assumes ideal environment, we can use the default setting which corresponds to no damping here.

Next come the boundary settings. For the gate structure examined here, it is a cantilever which means one end of the beam is fixed. As a result, we need to define some constrains to the left surfaces by changing the default boundary setting which is “free” to “fixed”.

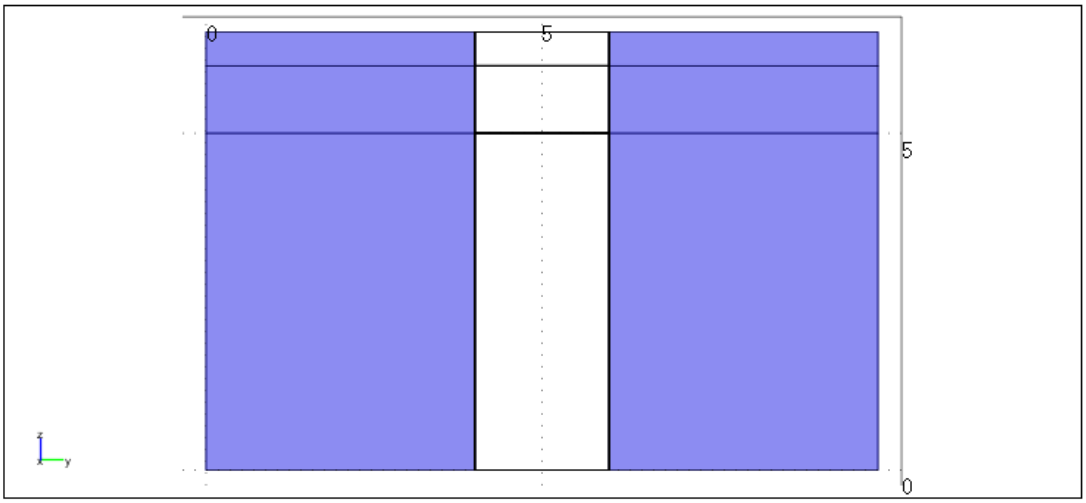

Figure 2.2.2 Side view of the cantilever from the fixed end. The surfaces in blue are fixed with zero degree of freedom while the rest white ones (air) are free.

Another thing to be considered under the Boundary settings is the load applied to the cantilever. In reality, a DC input magnetic signal modulated by a small AC signal will induce alignment of magnetic subdomains inside the magnetostrictive layer (Metglas layer). This will grant the Metglas layer magnet-like properties. The interaction between this induced magnet and the input signal contributes to the oscillation of the cantilever gate. Besides this, the small ac input magnetic signal will intrigue a tendency of the magnetostrictive layer to change dimensions. Then due to the bondings with the top and bottom layer, the tendency to change dimensions will manifest itself as an oscillatory movement of the cantilever. These two together result in the cantilever’s vibration which has been observed in experiments. However, since COMSOL

Multiphysics does not have a built-in module for magnetostriction, an alternative method was used in the simulation which is to model the situation by an equivalent force in z direction acting on the top surface of the simulated structure (shown as the blue in Figure 2.2.3).

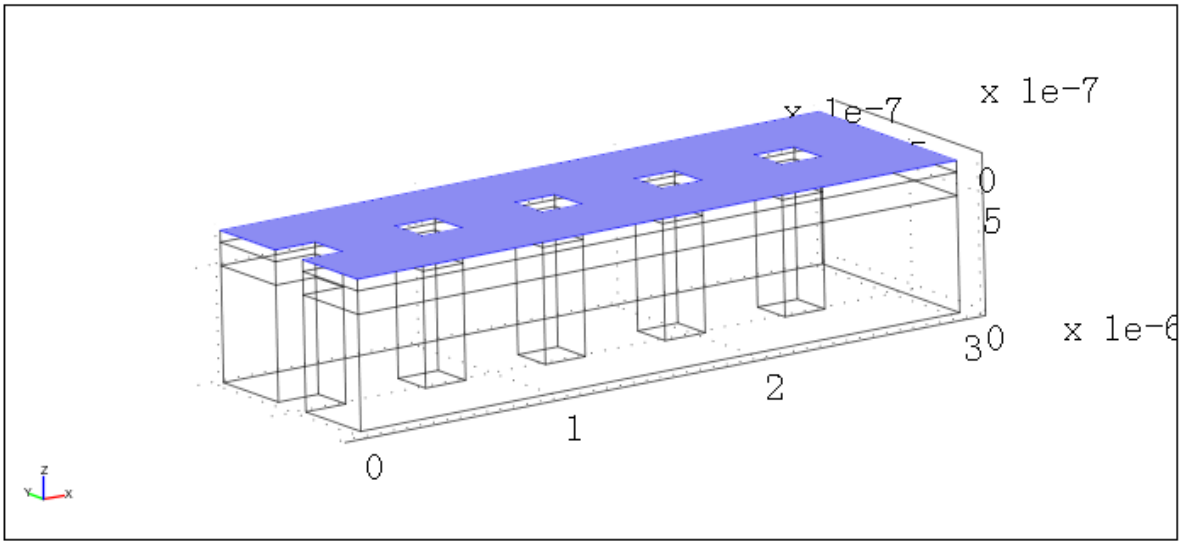

Figure 2.2.3 Cantilever gate with load applied to the top surface.

2.2.3 Simulation Results Analysis

Our interest here lies in the frequency response of the cantilever gate oscillation. That is to say, what we would like to analyze and compare with the experimental measurements is the response of the cantilever with input AC magnetic signal varying in frequencies.

As stated in section 2.2.2, the first case we were going to explore was when assuming ideal environment. With this assumption, we did not consider any initial stress in the three layers or air damping during the cantilever oscillation. As a result, the simulation should give a prediction of the designed cantilever's frequency response if the residual stress generated during thermal processes in fabrication can be eliminated and the device was operating in complete vacuum.

Using an analytical modal developed by Feng Li to calculate the equivalent force to apply to the cantilever's top layer during simulation, a value of $1.58\,N/m^2$ was obtained assuming the input AC magnetic signal to have amplitude of 0.38 Oe. With all the physical properties set up, before letting the simulator solve the problem, it was necessary to define mesh and frequency range of interest. After the assignment of solver parameters and waiting for the simulator to solve all the equations defining the scenario, the following results were obtained.

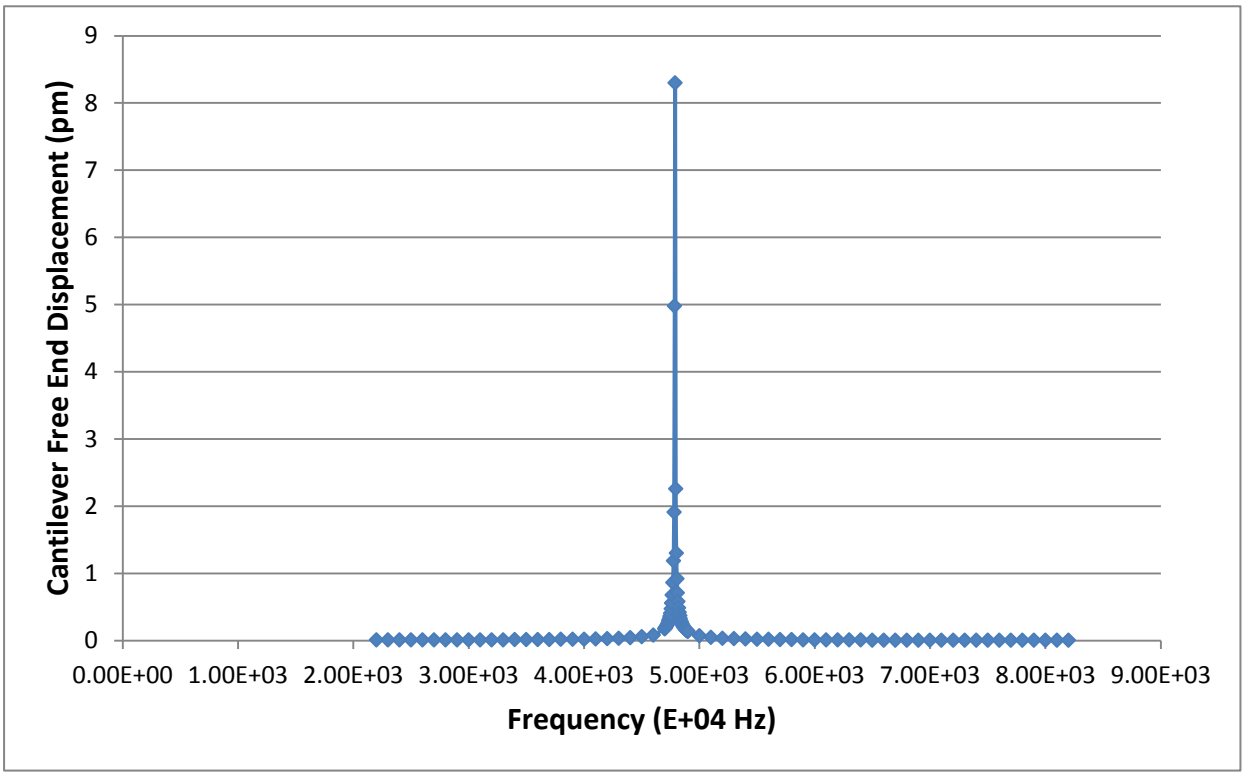

Figure 2.2.4 Frequency response (2.2e7 to 8.2e7 Hz) of the cantilever under ideal case. From the graph, the fundamental mode of resonance happens at 4.79e7 Hz with amplitude of 8.3 pm. The frequency sweep used in simulation is 2200e4:100e4:4700e4, 4700e4:5e4:4900e4, 4900e4:100e4:8200e4

One thing to be aware of is that since we scaled the width and length of the cantilever by 1/100 when doing simulations, we need to take into account the $\frac{1}{L^2}$ dependence of the cantilever resonant frequency on its length. Thus, dividing the results by 1e4, we can expect the actual cantilever gate to have a resonance frequency of 4.79 kHz.

The stress distribution as well as the cantilever displacement is showed below in Figure 2.2.5 (a) and (b).

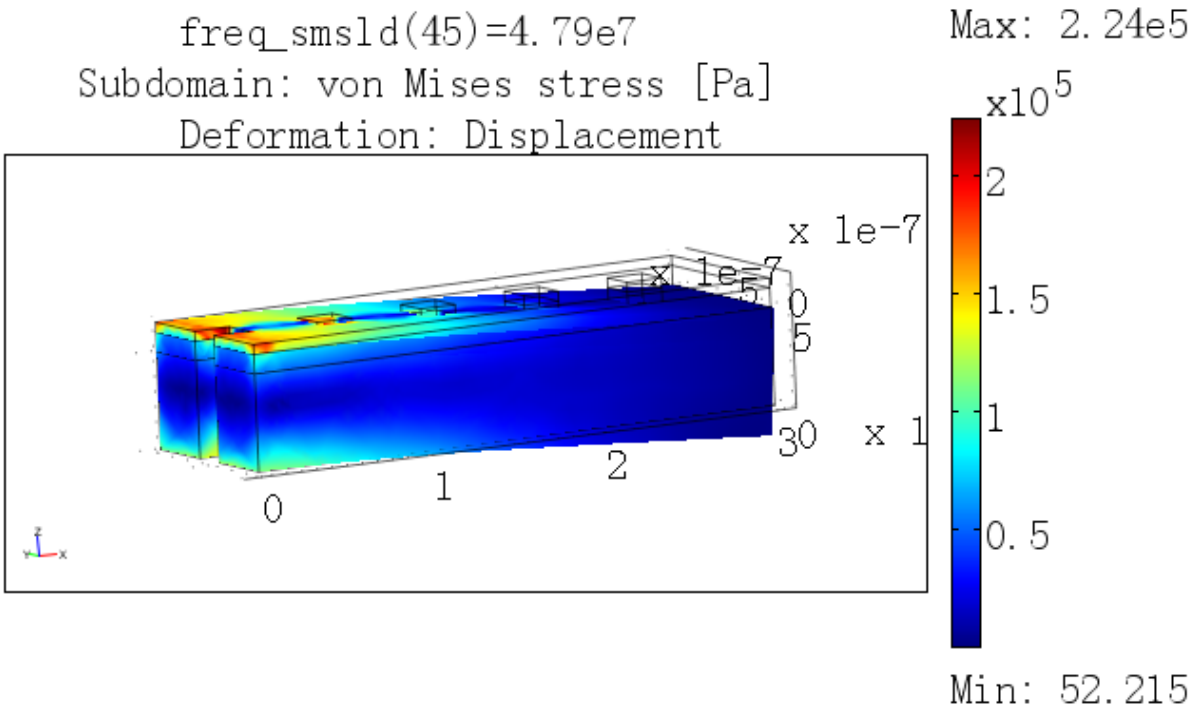

Figure 2.2.5 (a) Stress distribution in the cantilever at the resonance frequency under ideal case.

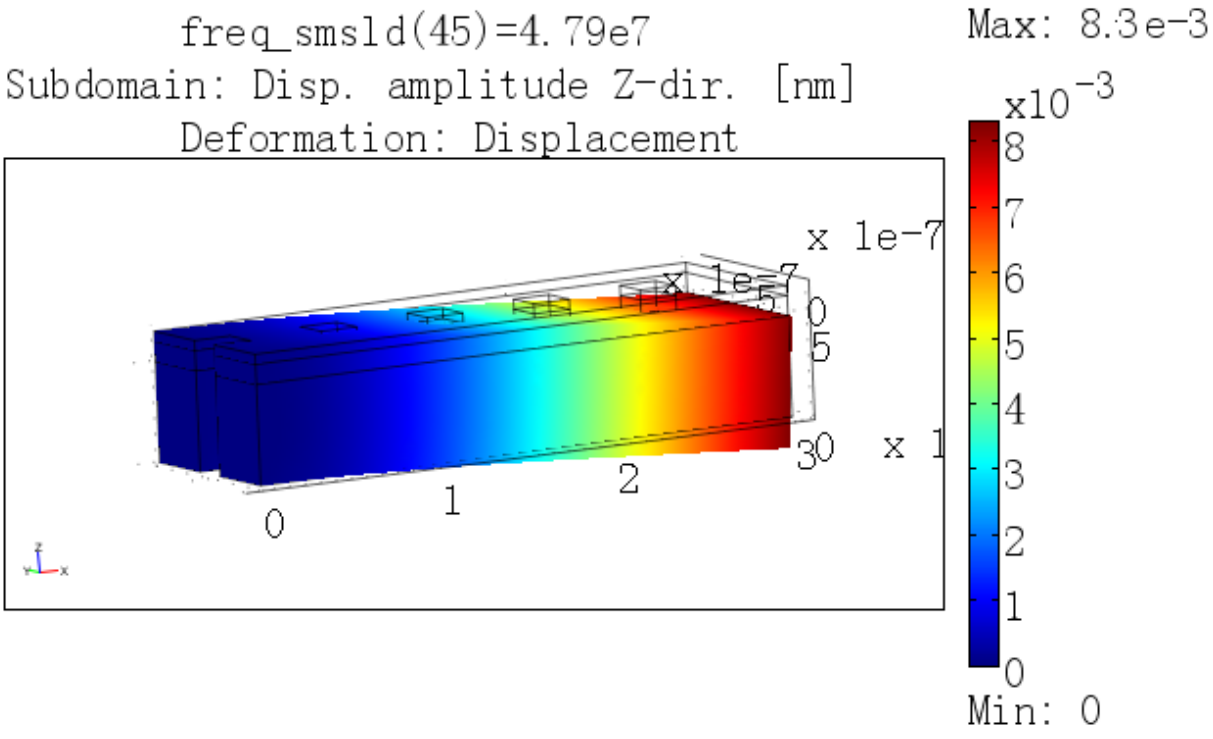

Figure 2.2.5 (b) Cantilever deflection at the resonance frequency under ideal case.

The above ideal case is not possible in reality since as mentioned in chapter 2.1.2, it is almost

impossible to eliminate residual stress due to various thermal processes during the cantilever fabrication. As a result, it is more practical to simulate the cantilever motion with the residual stress taken into account. Obtained from characterization of the fabricated devices, residual stresses mainly exist in the Metglas layer and the Titanium layer. The Metglas layer has a tensile residual stress of 100 MPa and the Titanium layer has a tensile residual stress of 200 MPa. To include these initial stresses, I modified the subdomain settings in COMSOL Multiphysics and obtained simulation results shown as below.

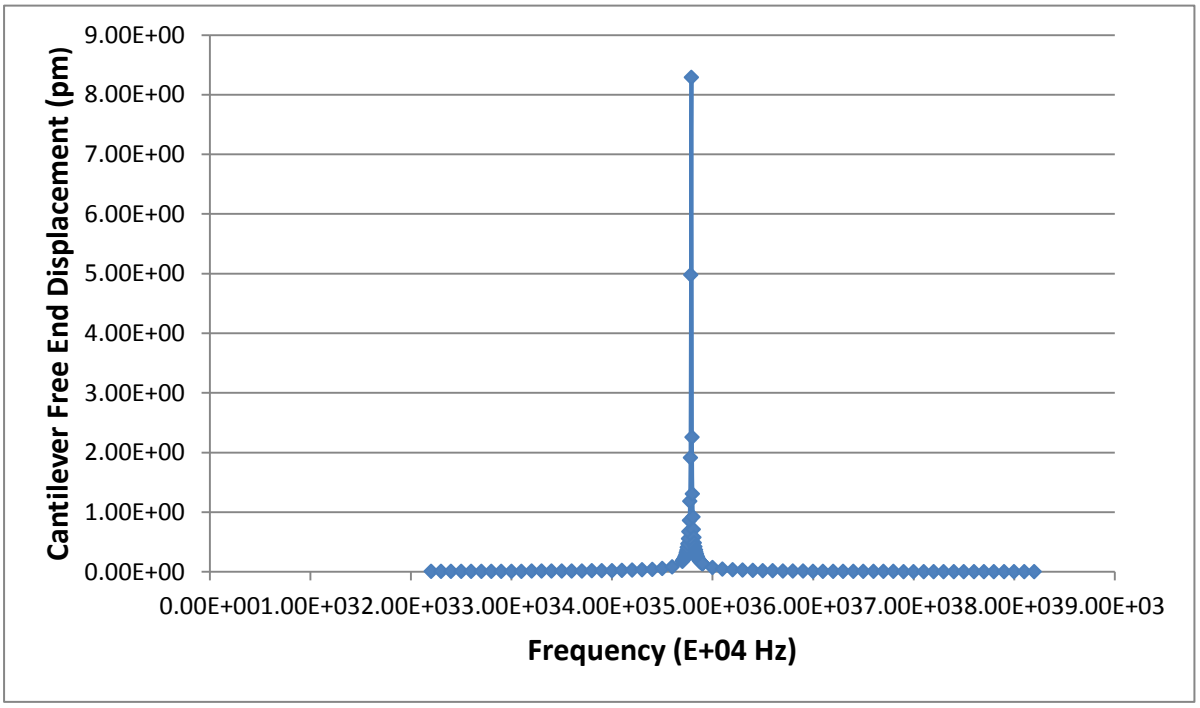

Figure 2.2.6 Frequency response (2.2e7 to 8.2e7 Hz) of the cantilever with residual stresses. From the graph, the fundamental mode of resonance happens at 4.79e7 Hz with amplitude of 8.29 pm.

Again, the stress distribution as well as the cantilever displacement is showed below in Figure 2.2.7 (a) and (b).

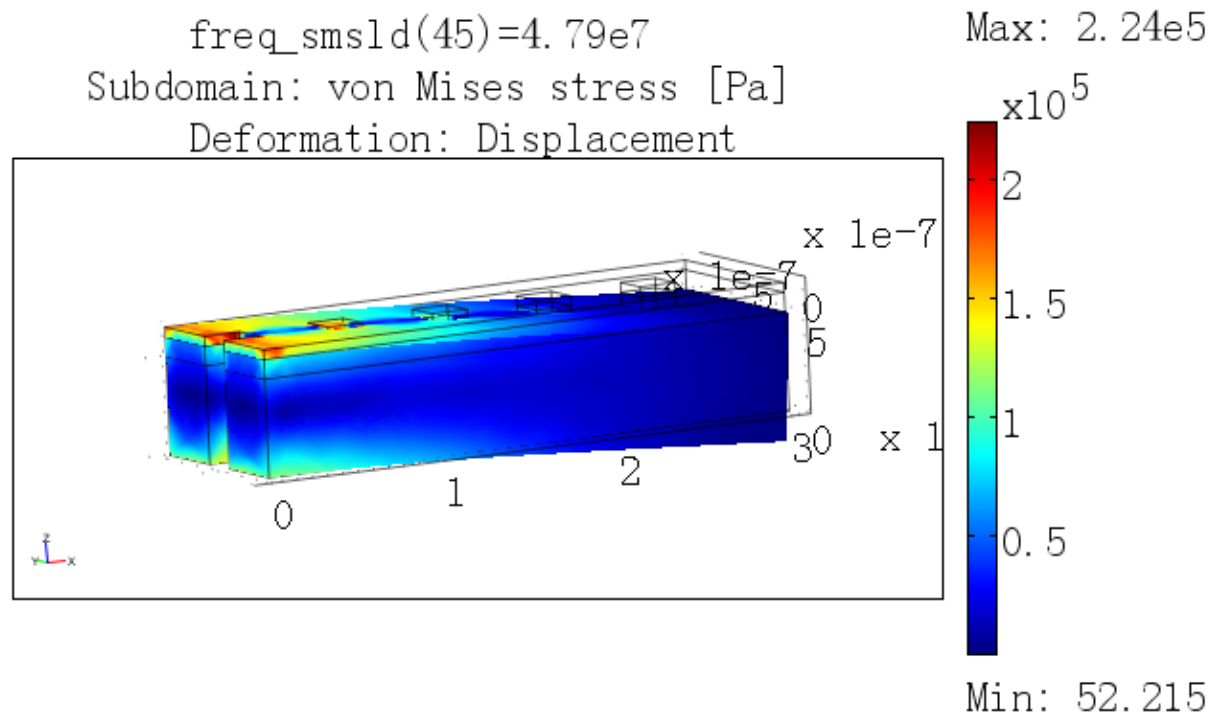

Figure 2.2.7 (a) Stress distribution in the cantilever at the resonance frequency with residual stresses taken into account.

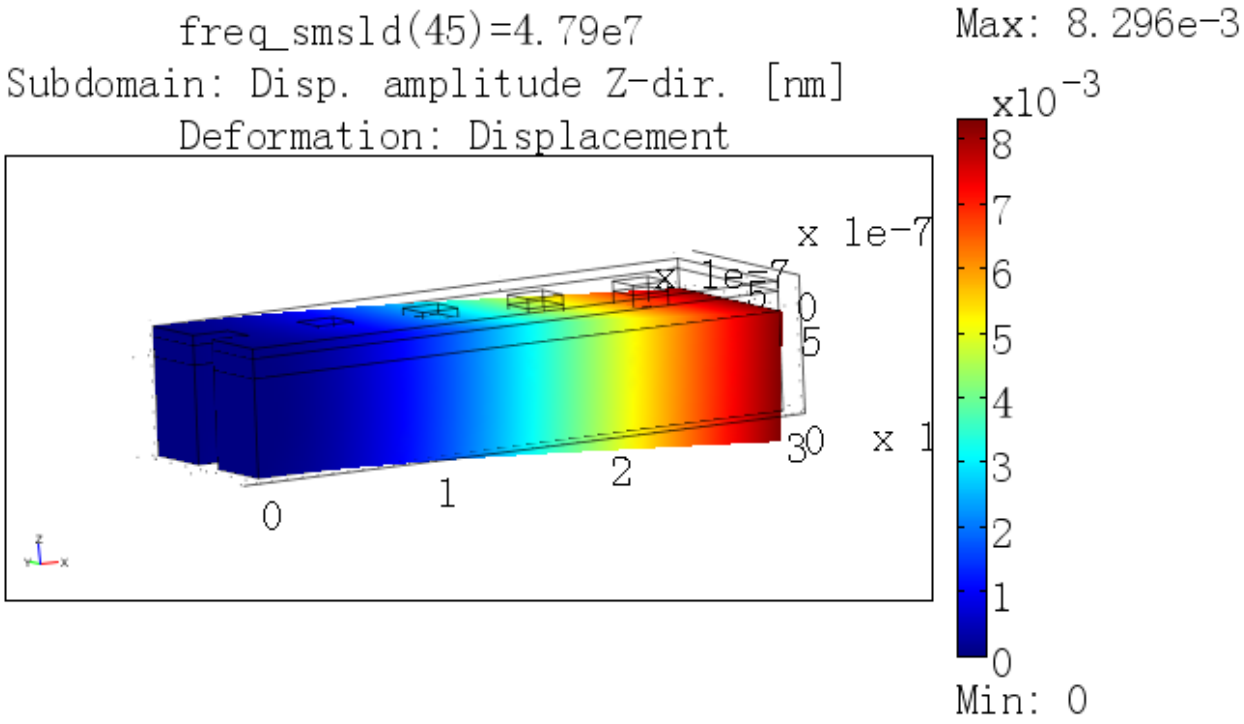

Figure 2.2.7 (b) Cantilever deflection at the resonance frequency with residual stresses taken into account.

Compared with results obtained under the assumption of ideal operating environment, we noticed that the maximum deflection amplitude decreases from 8.3 pm to 8.29 pm. This is because the residual stress makes the cantilever to have a larger stiffness and thus making it less easily to bend.

The next step was to consider the air damping effect. COMSOL Multiphysics supports two types of damping, the Rayleigh damping and the Loss Factor damping. Rayleigh damping modal assumes that the damping is proportional to a linear combination of the stiffness and mass. To calculate the stiffness and mass coefficients governing the amount of damping, one needs to specify two frequencies at which the object's performance is of interest. It has been shown that at those two specific frequencies, the simulations are pretty accurate. However, for all the other frequencies falling in between, there will be less damping than is in the actual case. Since in this thesis, the entire range of frequencies from 2200 Hz through 8200 Hz is of interest, the Loss Factor damping modal will better suit the purpose. As is usually the case for air damping, a loss factor of 0.01 has been chosen.

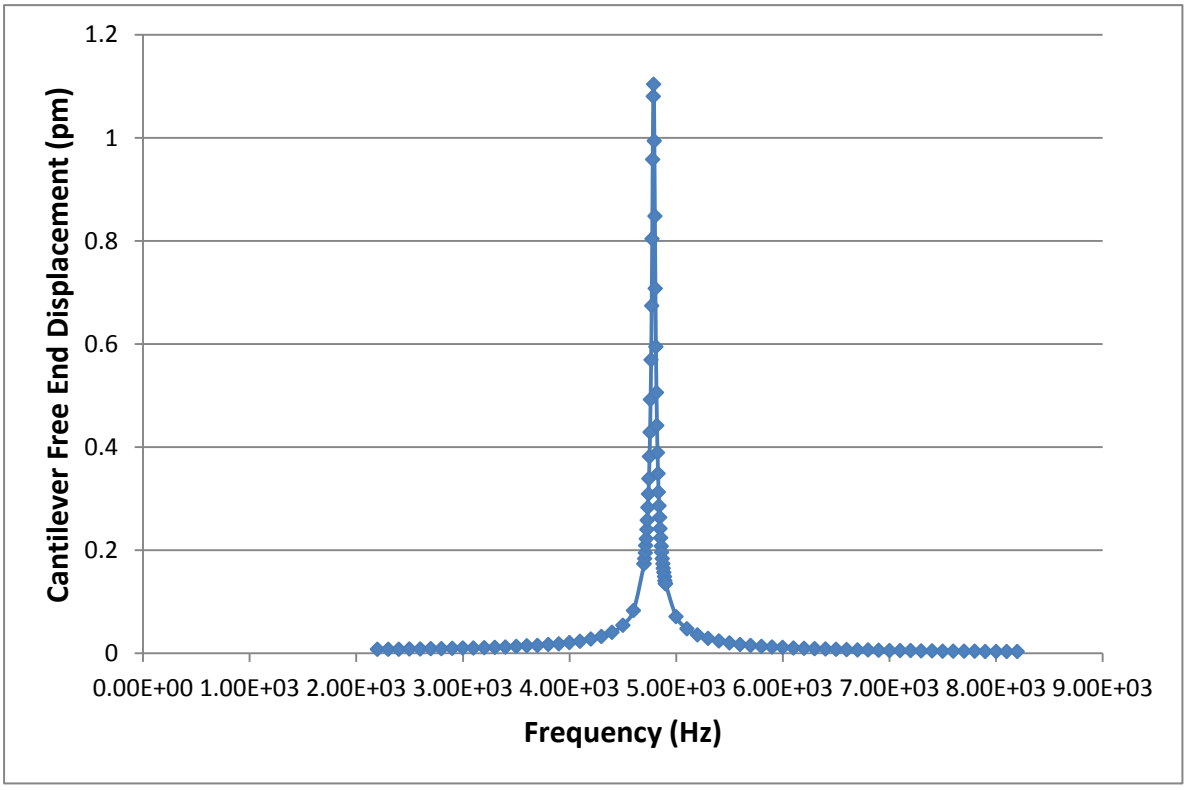

Figure 2.2.8 Frequency response (2.2e7 to 8.2e7 Hz) of the cantilever with residual stresses and a loss factor of 0.01. From the graph, the fundamental mode of resonance happens at 4.79e7 Hz with amplitude of 1.104 pm.

With all the simulation results, we can now compare the data with the experimental measurements. According to the experimental data, the cantilever resonance measured in vacuum (10^{-3} Torr) returns a resonance frequency of 4.8 kHz with a peak deflection of 8.893 pm. Recall that the simulation result suggests a resonance frequency of 4.79 kHz with a peak of 8.29

pm when no air damping effect is considered. The deviation of the simulation result from the measured one is mainly due to the discrepancies of material (mainly Metglas) related values defined in software simulation such as Young's modulus and Poisson's ratio of Metglas.

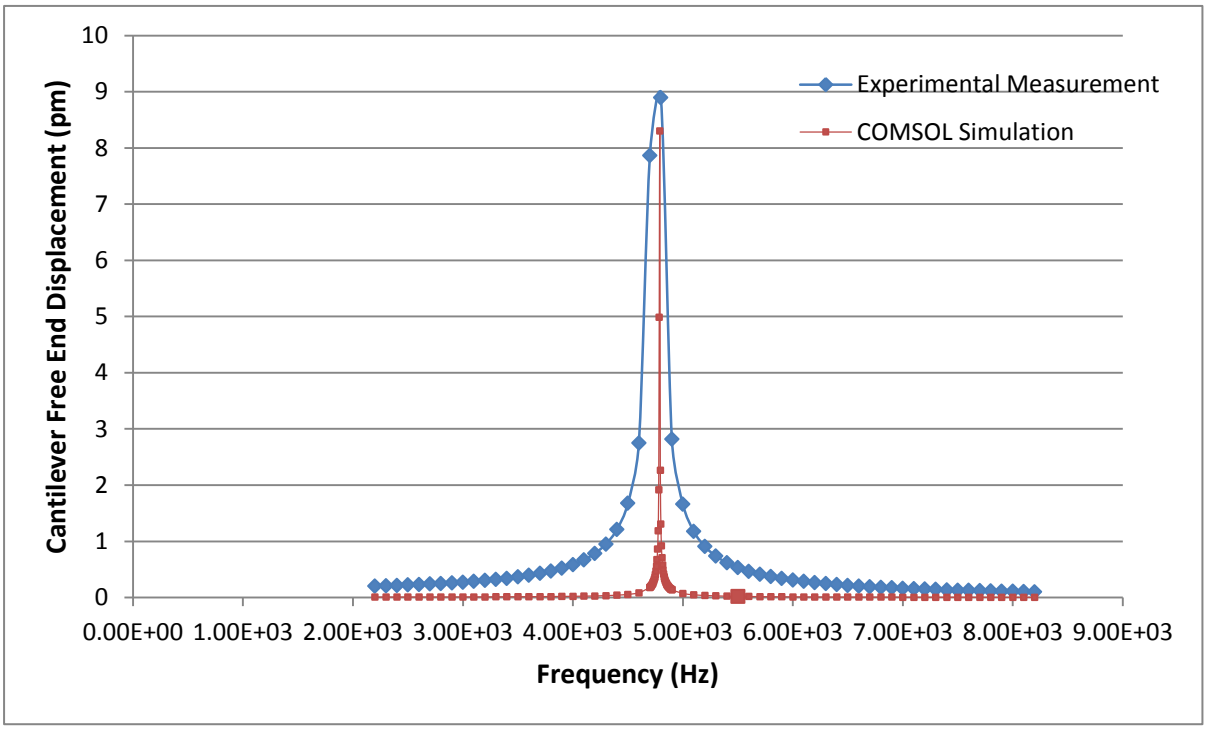

Figure 2.2.9 Comparison of the cantilever deflection measured in vacuum (0.3 Torr) and simulated without air damping effect included. Frequency response range is 2.2e7 through 8.2e7 Hz. From the graph, the fundamental mode of resonance happens at 4.8 KHz and 4.79 KHz with amplitude of 8.89 pm and 8.29 pm respectively.

2.3 CONSEDERATION FOR GATE REDESIGN

2.3.1 Redesign Process

In order to improve the sensitivity of the Titanium-Metglas-Platinum trimorph cantilever gate with respect to input AC magnetic signals, it is necessary to understand the physics behind the designed resonant gate and find out factors that may limit its sensitivity.

As mentioned before, the gate is composed of three layers made from titanium, metglas, and platinum from bottom to top. The metglas layer is the magnetostrictive layer which plays an extremely important role in the functioning of the MERGT. Due to the special property possessed by magnetostrictive materials, the metglas layer will tend to change its dimensions upon an applied magnetic signal. However, since the metglas layer is bonded to the other two layers at both its top and bottom surface, it is not free to change dimensions. As a result, the tendency of the metglas layer to stretch or shrink will manifest itself as either bending upward or downward. This is how the cantilever as a whole resonates in response to an AC magnetic signal. During the entire process, the magnetic flux generated inside the cantilever body upon an applied magnetic field will determine the extent to which the magnetostrictive layer want to change dimensions and thus is critical in determining the amplitude of the gate displacement. Also, the stiffness of the cantilever can determine the easiness for it to bend. As a result, we can conclude that in order to improve the sensitivity of the gate, we need to consider how the gate dimension is related to the generated magnetic flux and cantilever stiffness.

According to [9], magnetic flux concentration effect varies greatly with the metglas sheet aspect ratio. The simulation using COMSOL Multiphysics in [9] suggests that magnetic flux density at the central region of the metglas sheet in a magnetic field increase markedly as the sheet aspect ratio (width to length ratio) decreases, demonstrating almost 7 times increment as the aspect ratio decreases from 2/3 to 1/30. As a result, in order to have a larger flux density in the metglas sheet of the gate structure under a small AC magnetic field, smaller aspect ratio of the metglas sheet is desired.

However, merely taking into account the flux concentration effect is not enough. We should also study how the stiffness of the three-layer cantilever changes with gate dimensions. For a fundamental one-layer cantilever, Stoney's formula gives an accurate account of the cantilever deflection δ with respect to applied stress σ :

$$\delta = \frac{3\sigma(1-\upsilon)}{E}\left(\frac{L}{t}\right)^2$$

where υ is Poisson's ratio, E is Young's modulus, L is the cantilever beam length and t is the cantilever thickness. However, for the cantilever studied here, the deflection is not simply proportional to $\left(\frac{L}{t}\right)^2$ since the interaction between the three layers will add to the complexity of the structure as a whole. In addition, the magnetostrictive layer will also affect the stress

generated under a certain magnetic field. Many researches have been going on designing magnetostrictive sensors and among them is a work of Wetherhold and Chopra on beam model for calculating magnetostriction strains in thin film and multilayers [10]. Using the formula introduced in the paper, a MATLAB program (Included in Appendix A) has been developed to study the relationship between gate displacement and thickness ratios among the three layers.

Figure 2.3.1 below demonstrates the changes of gate deflection as a function of both $t_{titanium}/t_{metglas}$ and $t_{platinum}/t_{metglas}$.

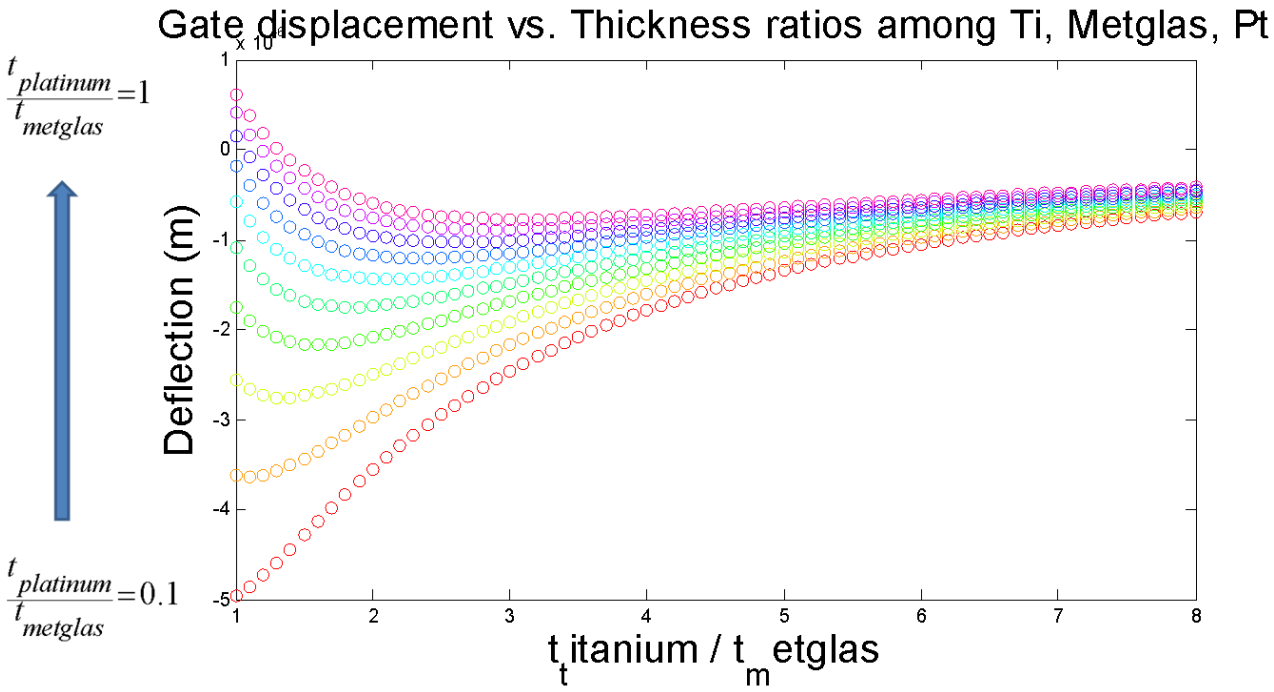

Figure 2.3.1 Presented in the plot are ten groups of data. From bottom to top, $t_{platinum}/t_{metglas}$ increases from 0.1 to 1 with a step of 0.1. The horizontal axis shows the change of $t_{titanium}/t_{metglas}$ from 1 to 8 with a step of 0.1.

According to the plot, we can see that as $t_{platinum}/t_{metglas}$ increases from 0.1 to 1 when $t_{platinum}/t_{metglas}$ is fixed, the gate deflection decreases. Similarly, if $t_{titanium}/t_{metglas}$ increases from 1 to 8 while $t_{platinum}/t_{metglas}$ remains fixed, the gate deflection increases but with a decreasing rate of change. To better show this, the rate of change is presented in Figure 2.3.2.

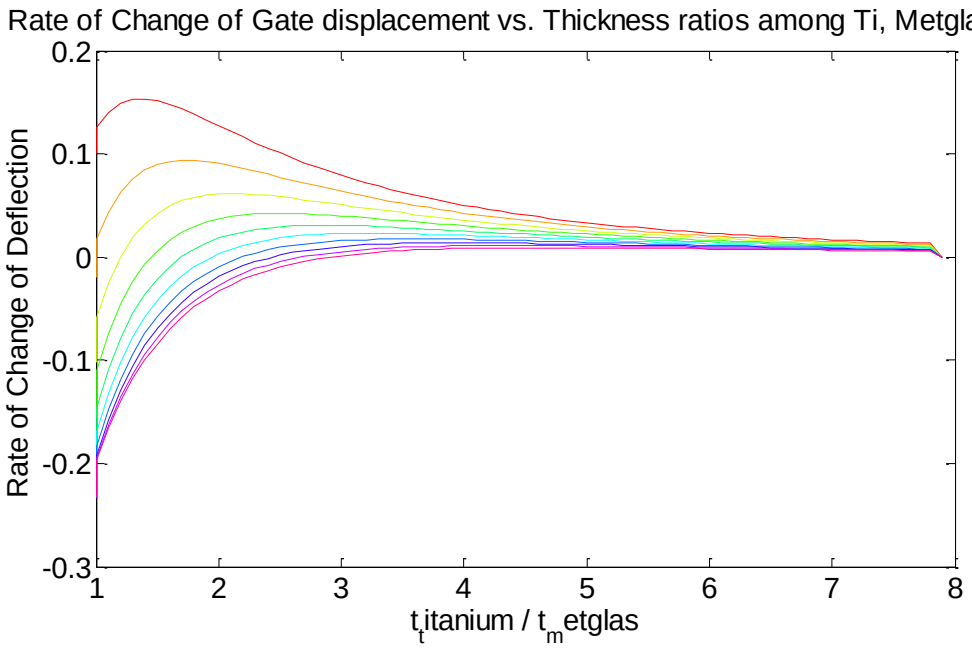

Figure 2.3.2 Rate of change of cantilever deflection

After knowing the dependence of cantilever deflection on thickness ratios among the three layers, we can now relate the cantilever deflection to the differential capacitance generated by the parallel gate capacitor with the top plate being the resonant gate and the bottom plate being a fixed gate pad residing on the nFET of the MERGT. According to [11], a MATLAB program (Appendix A) was written to study the change of differential capacitance with the change of thickness ratios as well as the cantilever deflections. Then the data of interest was exported to an excel file and plotted as shown below in Figure 2.3.3.

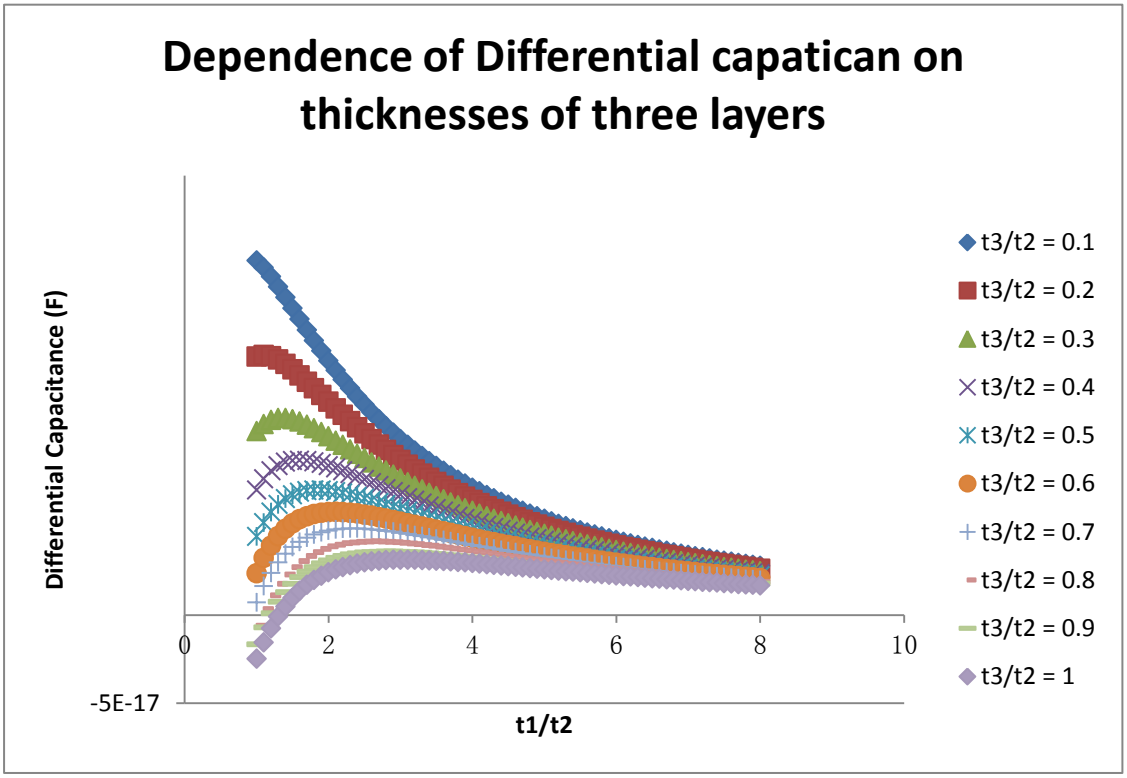

Figure 2.3.3 t1, t2, and t3 represent the thicknesses of the titanium, the metglas, and the platinum layer respectively.

The above plots are obtained under the assumption that the cantilever length and width are fixed at $300\mu m$ and $100\mu m$. Under such scenario, we would want to make the top and bottom layers as thin as possible. However, in reality, due to thermal processes during the fabrication and the fact that the three materials have different thermal expansion coefficients, the actual cantilever will not be flat at rest. Then cantilever tip would bend up a little due to the mismatch of tensile residual stress in mainly the middle and bottom layers. Considering this, we would want to make the titanium layer thick enough so that the initial bending of the cantilever is minimized. To balance between the two considerations, I have proposed a cantilever design with modified Pt and Ti thicknesses.

	Titanium	Metglas	Platinum
Thickness (nm)	300	100	30
Position	Bottom	Middle	Top

Table 2.3.1

With these new values, the next step is to consider what the optimal length and width values should be. A MATLAB program (Appendix B) has been written to achieve this.

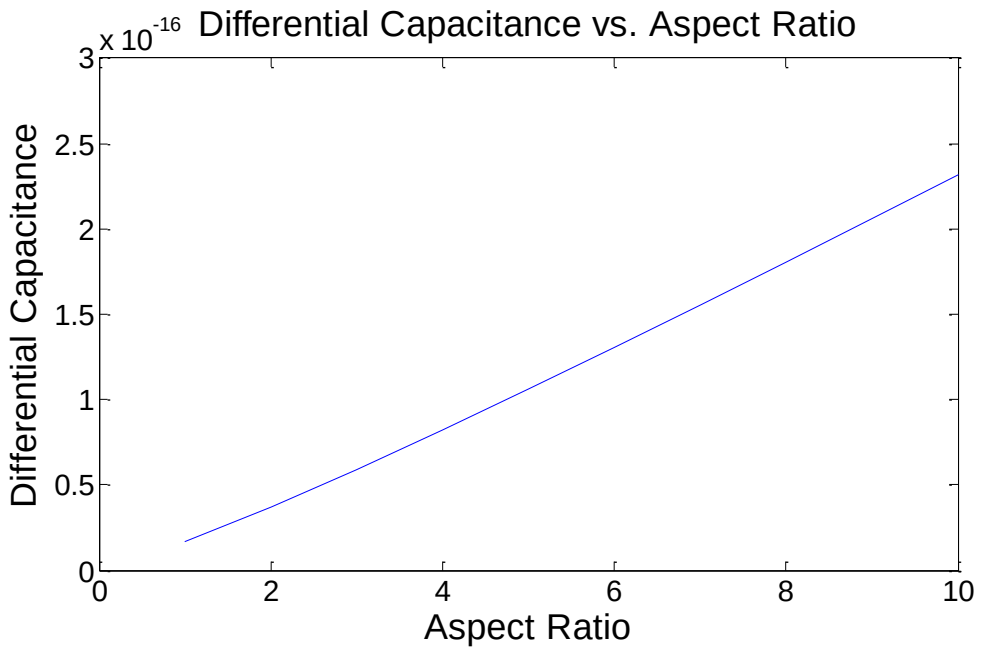

Figure 2.3.4 shows how the differential capacitance (in Farad) changes as the aspect ratio (length to width ratio) increases from 1 to 10.

From Figure 2.3.4, we can see that, the differential capacitance-aspect ratio relationship is almost linear. However, if we increase the aspect ratio too much, then the air gap between the resonance gate and the underlying gate pad will increase substantially. This means that air

damping may become a very significant issue. Also, due to the consideration for IC monolithic process fabrication, we would like to keep the dimensions of the device small. Taking all these into account, a complete new gate structure is proposed as below.

	Titanium	Metglas	Platinum
Length (um)	500	500	500
Width (um)	100	100	100
Thickness (nm)	300	100	30
Position	Bottom	Middle	Top

Table 2.3.2

2.3.2 Simulation Verification with COMSOL Multiphysics

Instead of building the new cantilever gate immediately, software simulation will be conducted to verify the feasibility of the design.

Due to the same reason as stated in section 2.2, the structure actually being simulated is

	Titanium	Metglas	Platinum
Length (um)	5	5	5
Width (um)	1	1	1
Thickness (nm)	300	100	30
Position	Bottom	Middle	Top

Table 2.3.3

where the cantilever length and width are again scaled by 1/100.

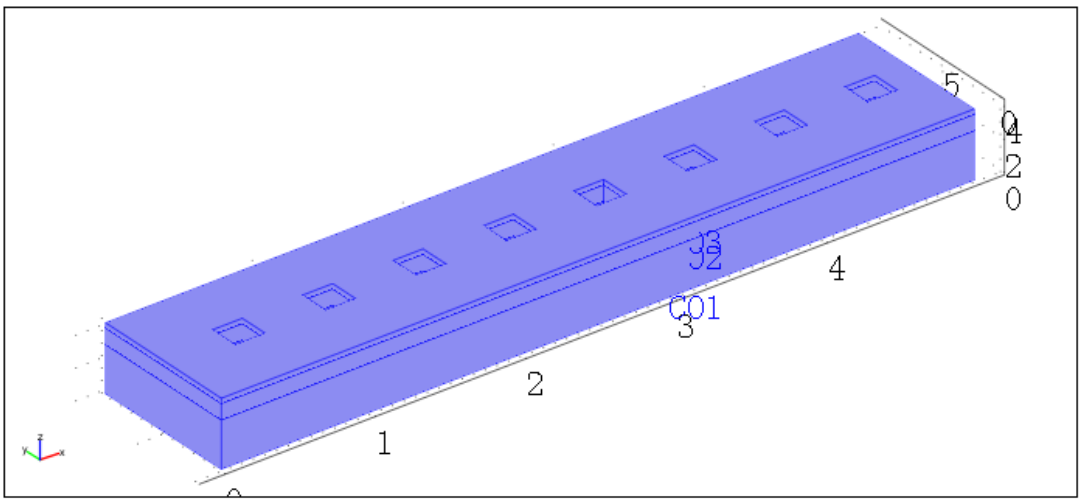

Figure 2.3.5 Geometry of the newly designed cantilever gate built in COMSOL Multiphysics.

In order to compare the sensitivity of this newly designed gate with the old one, all the subdomain and boundary settings are the same with those defined for the old cantilever. As we can see in Figure 2.3.6, the equivalent driving force is applied to the top surface of the simulated

cantilever structure as what has been carried out in the cantilever movement simulation with the original dimensions.

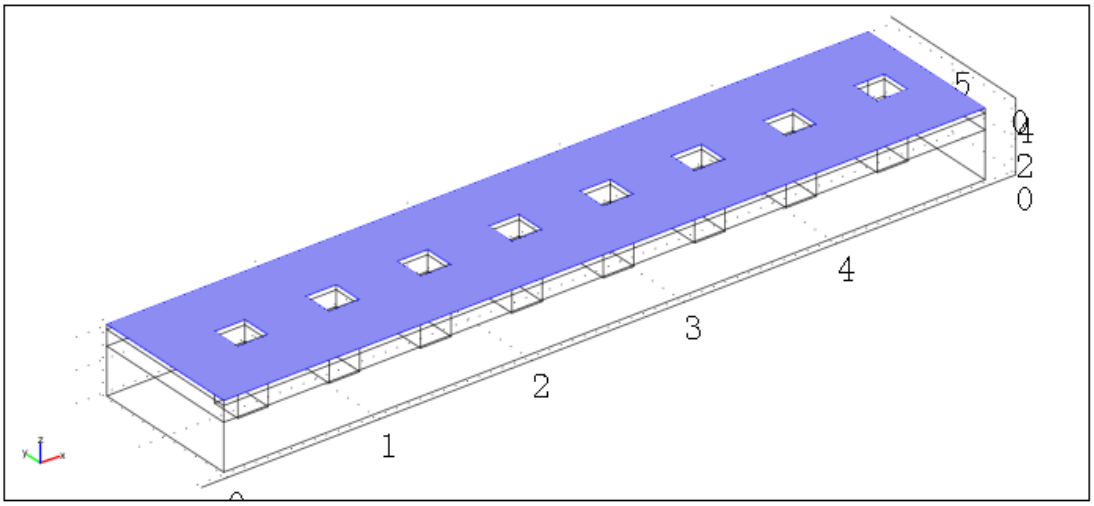

Figure 2.3.6 Load applied to the top surface of the newly designed cantilever.

The resulted frequency response of the cantilever as well as the stress distribution and displacement are shown below.

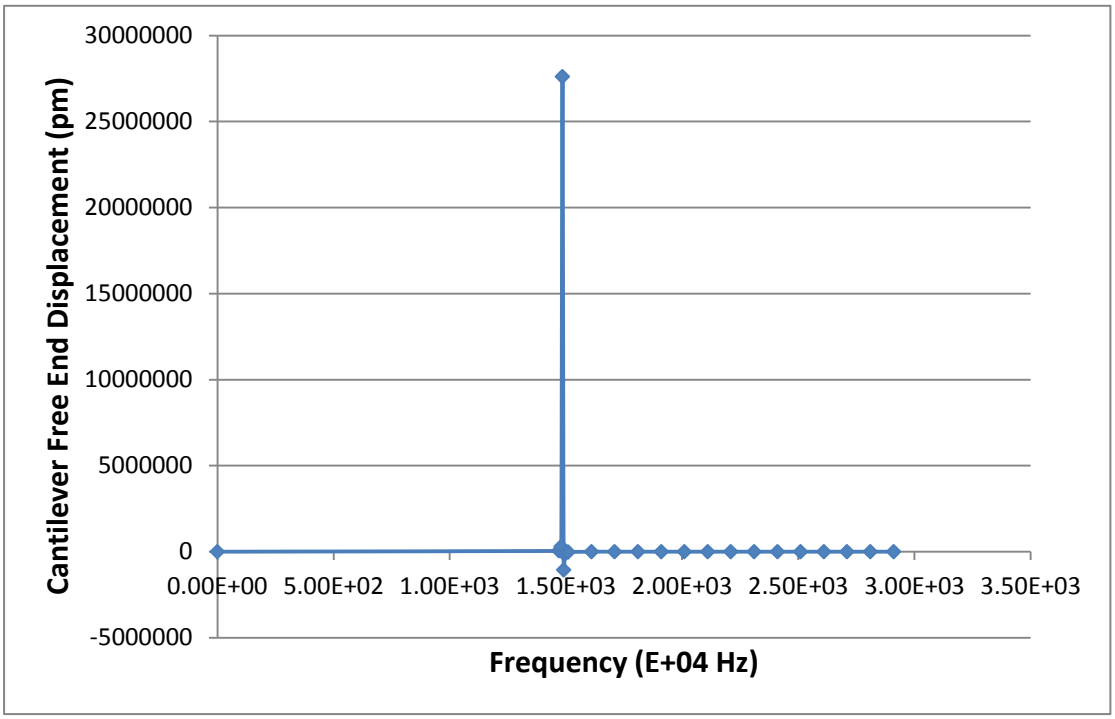

Figure 2.3.7 Frequency response (0 to 3e7 Hz) of the cantilever under ideal case. From the graph, the fundamental mode of resonance happens at 1.485e7 Hz with amplitude of 27606266.7 pm.

This enormously large deflection at resonance frequency is unrealistic since the cantilever would have clamped into the underlying gate pad. However, the result indicates an improved deflection compared with the original device. Also, considering the influence of the air damping on the

oscillating cantilever, it is impossible to obtain such high deflection magnitudes in any real application. Even if we try to assure that the functioning environment of the cantilever is in “vacuum”, it is still not the absolute vacuum assumed by the software solver. Under this big picture, I included one more defining function into the COMSOL Multiphysics model which is called “Loss Factor Damping” under the damping tap of subdomain settings. For the case studied here, the resonance vibration is at low kHz range, so the main type of damping of importance is viscous damping. This type of damping is originated from energy dissipation occurring when mechanical systems oscillate in a fluid medium, such as air, gas, water and oil. As previously did, I used a loss factor of 0.01 to account for the opposing force imposed on the cantilever by air. With all the other settings same as the ideal cases, the newly designed cantilever returned the following simulation result.

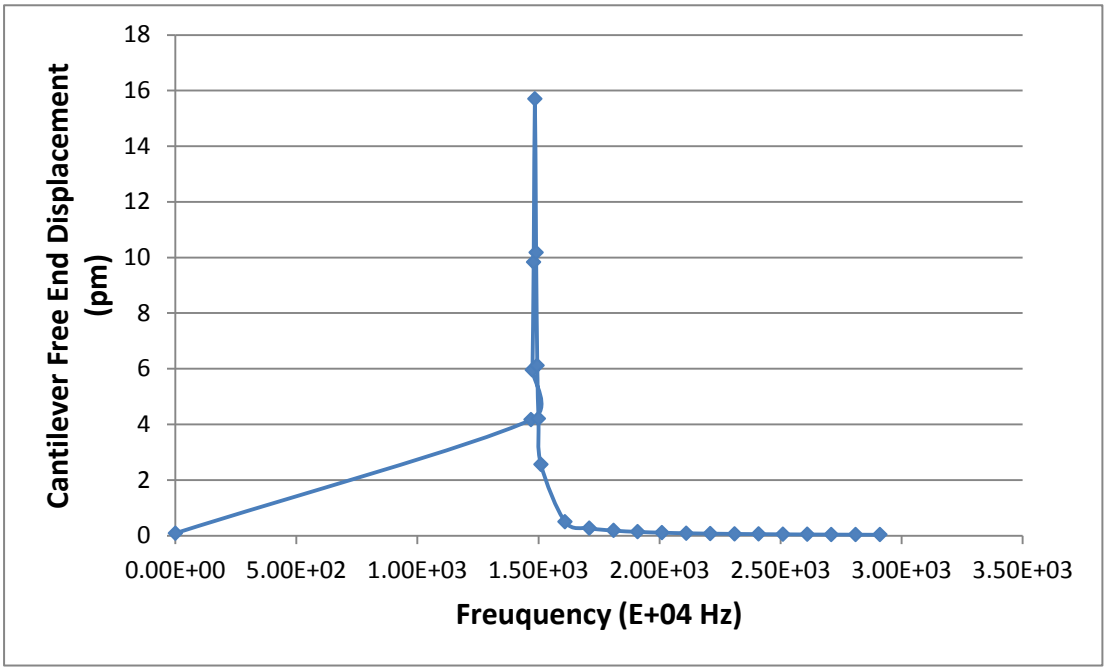

Figure 2.3.8 Frequency response of the newly designed cantilever structure under air damping with loss factor = 0.01

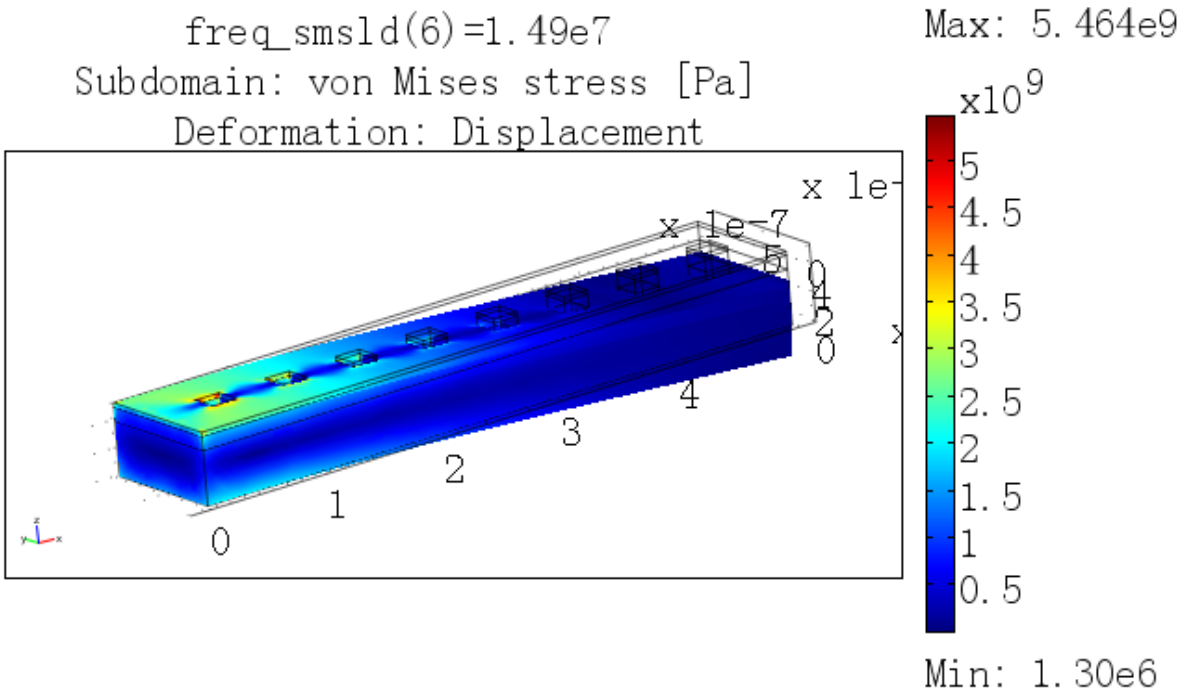

Figure 2.3.9(a) Stress distribution within the gate cantilever at a resonance frequency of 1.485e7.

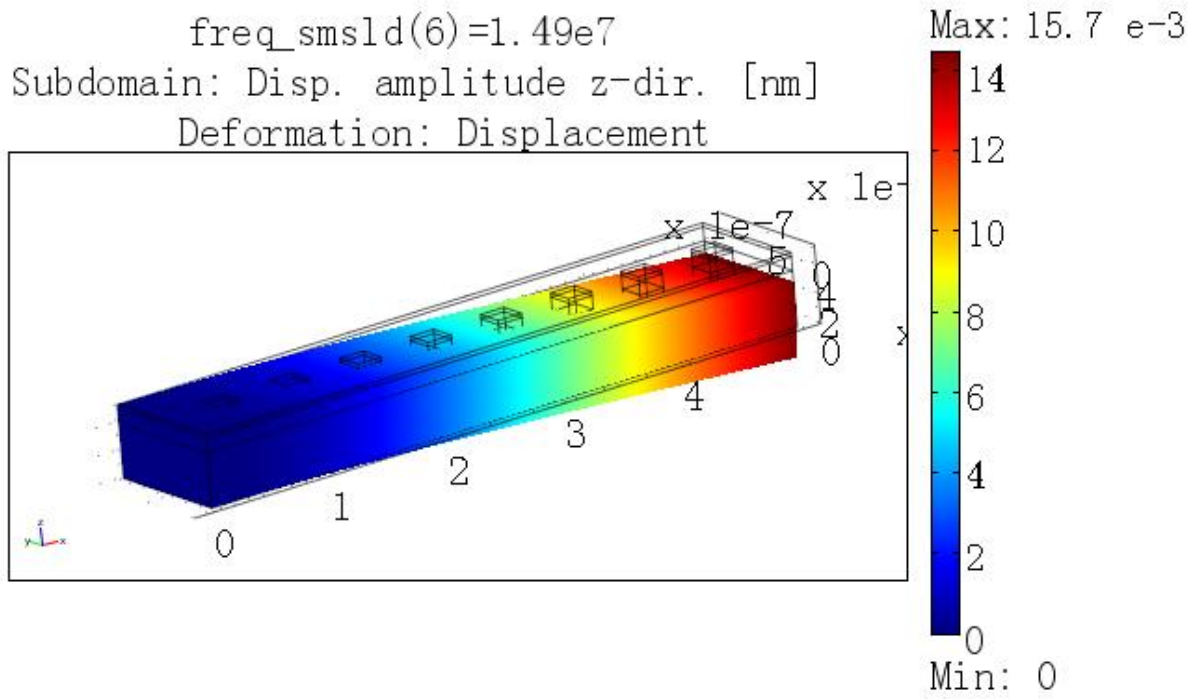

Figure 2.3.9(b) Cantilever gate displacement at a resonance frequency of 1.485e7.

Shown by the simulation result, we can see that the peak deflection magnitude now is 15.7 pm and happens at 1.485e7 Hz (Keep in mind the fact that modal used in simulation has a length and

width scaled by 1/100 compared with the actual design. This means that 1.485e7 Hz returned by simulation indicates 1485 Hz in reality).

Recall that before taking into account the air damping effect, the simulation results indicate a peak deflection magnitude of 27606266.7 pm. Comparing with the 15.7 pm obtained with a loss factor of 0.01, we can see that air damping plays a much more important role in the functioning of this newly designed cantilever. Since the air damping has dependence on the total area susceptible to the opposing force brought about by air, this huge deduction in peak deflection is within expectation.

Chapter 3

SIMULATION OF THE DESIGNED N-CHANNEL FIELD-EFFECT-TRANSISTOR

3.1 2-D n-Channel Field Effect Transistor

3.1.1 A Brief Overview of TCAD Sentaurus

TCAD is short for Technology Computer-Aided Design and is used to simulate the development and optimization of semiconductor processing technologies and devices. TCAD simulation tools solve fundamental, physical, partial differential equations. This physical approach gives TCAD simulation predictive accuracy. Therefore, it is possible to substitute TCAD computer simulations for costly and time-consuming test wafer runs when developing and characterizing a new semiconductor device or technology. TCAD consists of two main branches: process simulation and device simulation. Process simulation deals with processing steps such as etching, deposition, ion implantation, thermal annealing, and oxidation while device simulation solves for the electrical behavior of a semiconductor device. In this thesis, the main components of TCAD Sentaurus used are Sentaurus Structure Editor, Sentaurus Device and Tecplot.

3.1.2 2-D Structure Construction in Sentaurus

For the purpose of this thesis, the start with Sentaurus software simulation was to build the 2-D MOSFET geometry and define the doping concentrations of different regions in the transistor. To realize this, Sentaurus Structure Editor was used where the 2-D device model was created geometrically in the graphical user interface (GUI). Unlike the novel resonant gate, the n-channel field effect transistor used is a standard and well developed micro-scale MOSFET. The entire transistor is an n-type (Phosphorous as dopant) enhancement mode transistor with a p-type (Boron as dopant) Silicon substrate, and a Silicon Dioxide gate oxide. The channel length of the MOSFET is 10 μm and the gate oxide thickness is 22 nm. The source and drain region extend with lengths of 10 μm. The doping profile of the source and drain region are Gaussian with a peak concentration of 3e19 and a junction depth of 0.5 μm. After completing the construction of the device geometry in GUI as well as completing doping profile assignments, mesh profile needed to be defined to enable computer to solve related governing equations at specific points in the model. When doing mesh assignments, several factors need to be considered simultaneously in order to achieve a balance between the solution resolution and time required for the computer to conduct calculations.

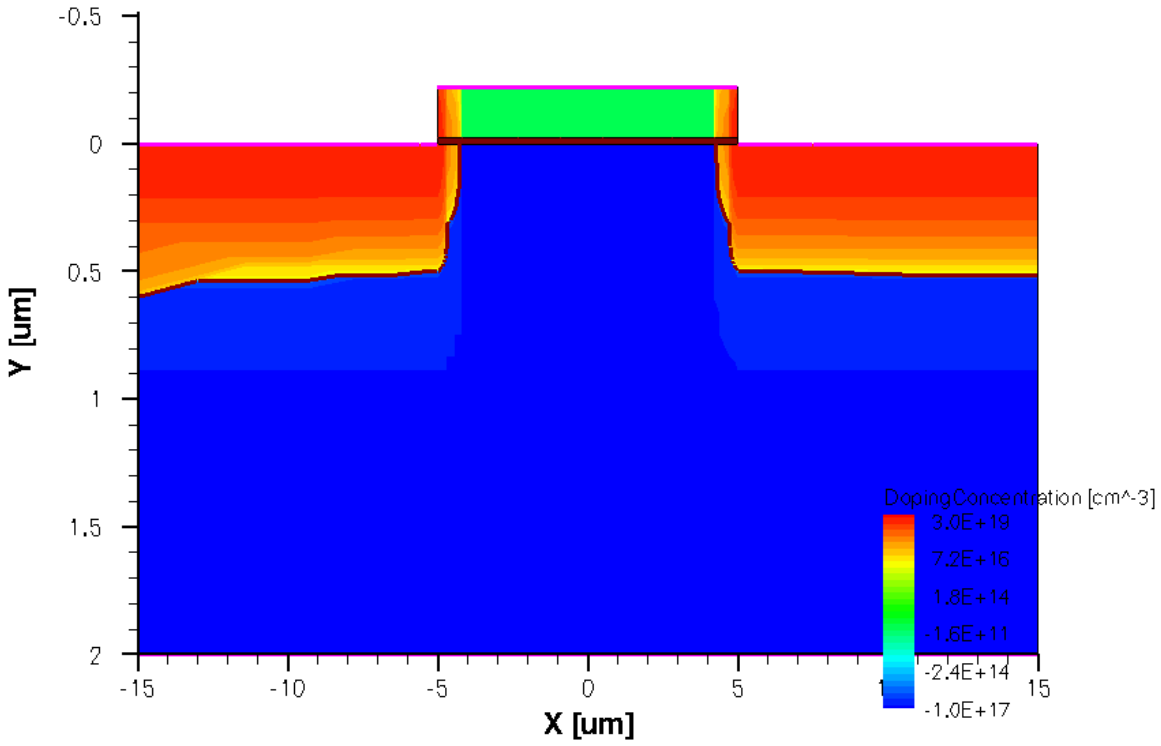

Figure 3.1.1 (a) Doping profile of the n-channel field-effect-transistor

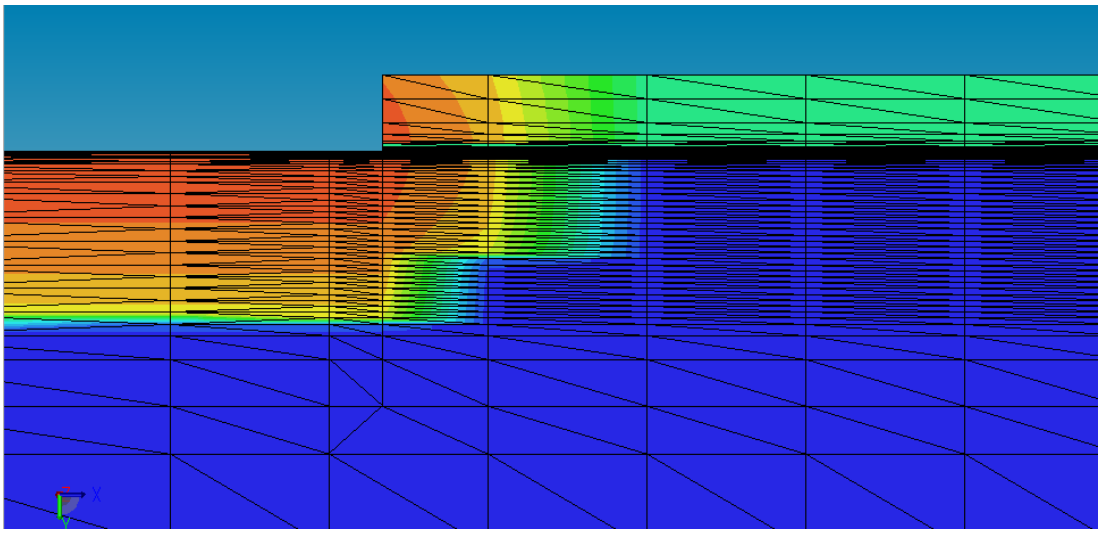

Figure 3.1.1 (b) Demonstration of the mesh profile defined for the device near source and gate interface region.

With the successful meshing of the model, the next step was to utilize Sentaurus Device to simulate the Id-Vg characteristics of the model. Sentaurus Device is a numeric semiconductor device simulator, capable of simulating the electrical, thermal, and optical characteristics of various semiconductor devices. One special characteristic of Sentaurus Device is that it requires script files to define all the physical properties of the device and solution approaches instead of the user interface format used in COMSOL Multiphysics. Such script file is called a command file. It includes 6 sections which are: file section, electrode section, physics section, plot section, math section, and solve section.

3.2 Simulation Result

3.2.1 Basic MOSFET Id-Vg Characteristic

As studied in previous chapters, the cantilever gate of the MERGT will respond to a magnetic signal and oscillate with a frequency same as the small magnetic field to be sensed. Besides the resonant cantilever gate, the MERGT also has an extended gate pad on top of the n-channel field effect transistor. The way this cantilever gate and the underlying gate pad work is similar to a parallel plate capacitor. From the basic formula $C = \frac{\varepsilon A}{d}$, we can expect the capacitance between the oscillating gate and the gate pad to change as the distance between them changes. In this way, the motion of the cantilever will affect the air-gap capacitance. With a fixed voltage Vg applied to the gate, the total charge stored in the FET gate region will change according to $Q = CV$. And lastly, this air-gap modulation will be amplified by the FET transconductance and present itself in the form of drain current modulation.

Now, after having understood how the n-channel field effect transistor manage to sense the cantilever gate motion, I would simulate the output drain current which reacts in response to a change in the channel charge density. Since there is some disconnection between the COMSOL Multiphysics simulation of the gate motion and the Sentaurus Device simulation of the n-channel field-effect-transistor, an analytical model [12] developed by graduate student Feng Li was used to calculate the variance of channel charge density from the cantilever deflection. The MATLAB m-file conducting the calculation can be found in Appendix C. Assuming the amplitude of the AC magnetic field to be 3 nT (the minimum AC magnetic field to have been detected in experiment), the analytical calculation returns a differential channel charge of 1.8790e-018 Colum.

The RGT was simulated using the 2-D NMOSFET structure developed with an added varying channel charge concentration condition. The MOSFET width of 100 μm is specified in physics section of the command file to overwrite the default value of 1 μm assumed for any 2-D structure in Sentaurus Device. The simulation result showing the MOSFET Id-Vg relationship is presented below and the command file is included in Appendix D.

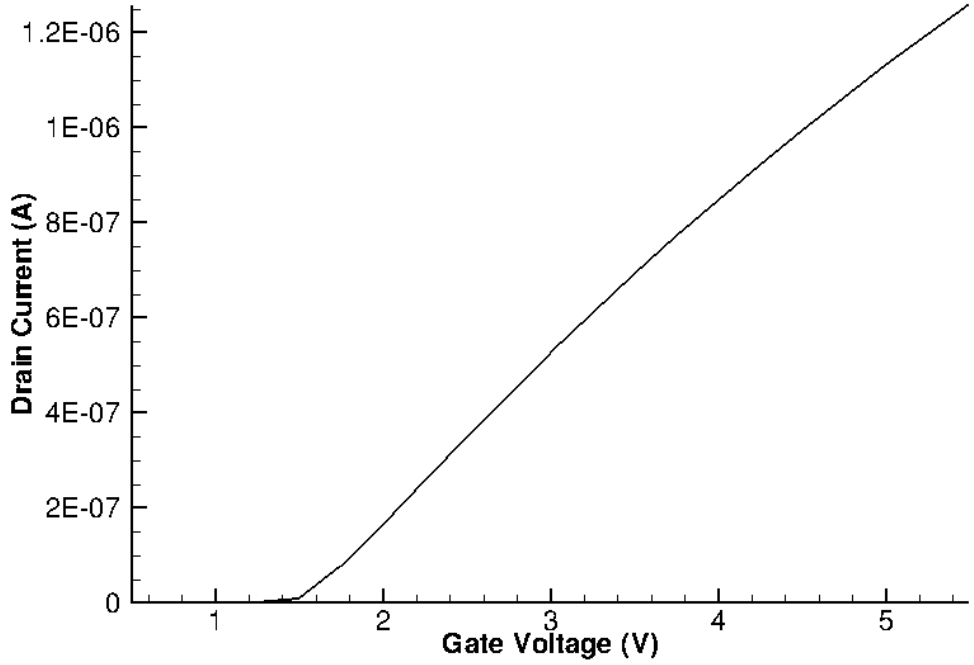

Figure 3.2.1(a) Id-Vg characteristic of the n-channel field-effect-transistor with $V_{ds} = 0.05V$ and V_{gs} spanning from 0V to 5V. From the plot, we can notice that the transistor threshold voltage is $V_{th} = 1.5V$.

To verify the electrical properties of the n-channel field-effect-transistor built with Sentaurus Structure Editor and simulated with Sentaurus Device, the Id-Vg characteristic obtained from both experimental measurement and simulation are compared below.

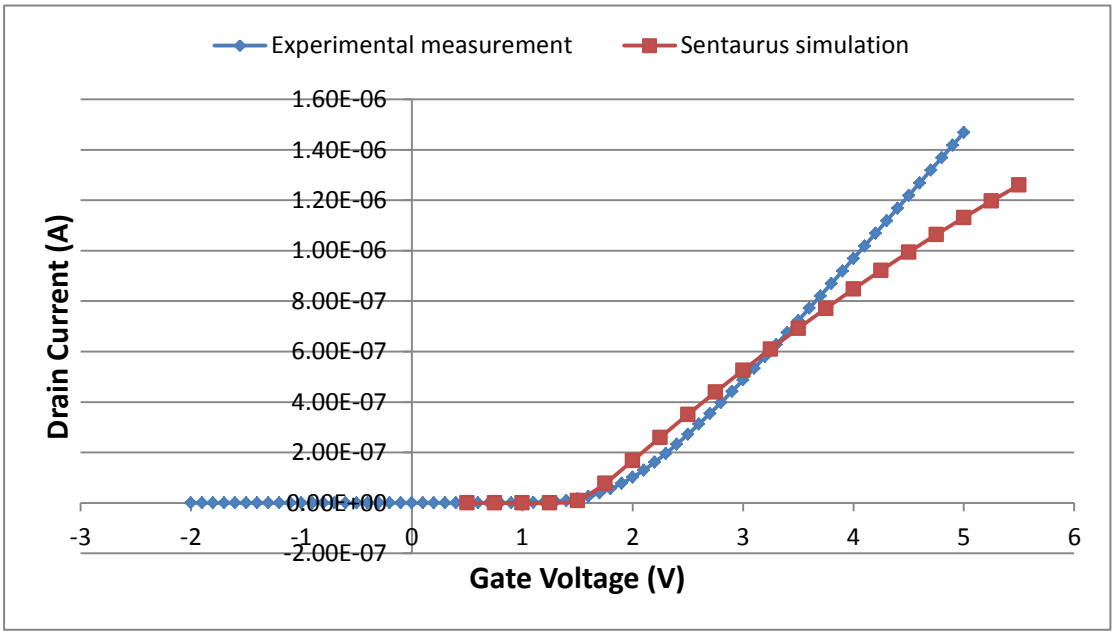

Figure 3.2.1(b) Comparison of Id-Vg characteristics.

From the above plot, we can see that the experimental measurement and simulation matches well. The small deviations may be due to some non-ideal physical conditions in the actual device such as fixed gate charges and impurity of materials.

3.2.2 NMOSFET Response with Varying Gate Charge

When the gate charge concentration of the MOSFET varies, the threshold voltage of the transistor will also change accordingly. This in turn results in changes of the total drain current. In theory, by detecting the change in output drain current, we should be able to sense the cantilever oscillation. However, since current is not easy to detect, it would be easier if a common source configuration is used to convert the drain current response to a voltage response. Considering this, instead of using the configuration in Figure 3.2.2(a), the one in Figure 3.2.2(b) was simulated. The command file specifying the simulation is shown in Appendix E.

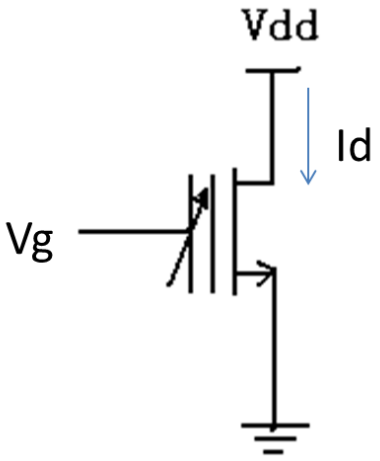

Figure 3.2.2(a) MERGT biased in saturation

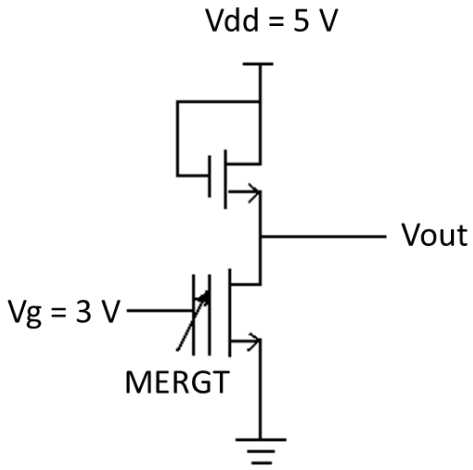

Figure 3.2.2(b) MERGT connected in a common source configuration

With the gate charge being a sinusoidal function with a frequency of 100 Hz, the output voltage V_{out} also varies sinusoidally with the same frequency.

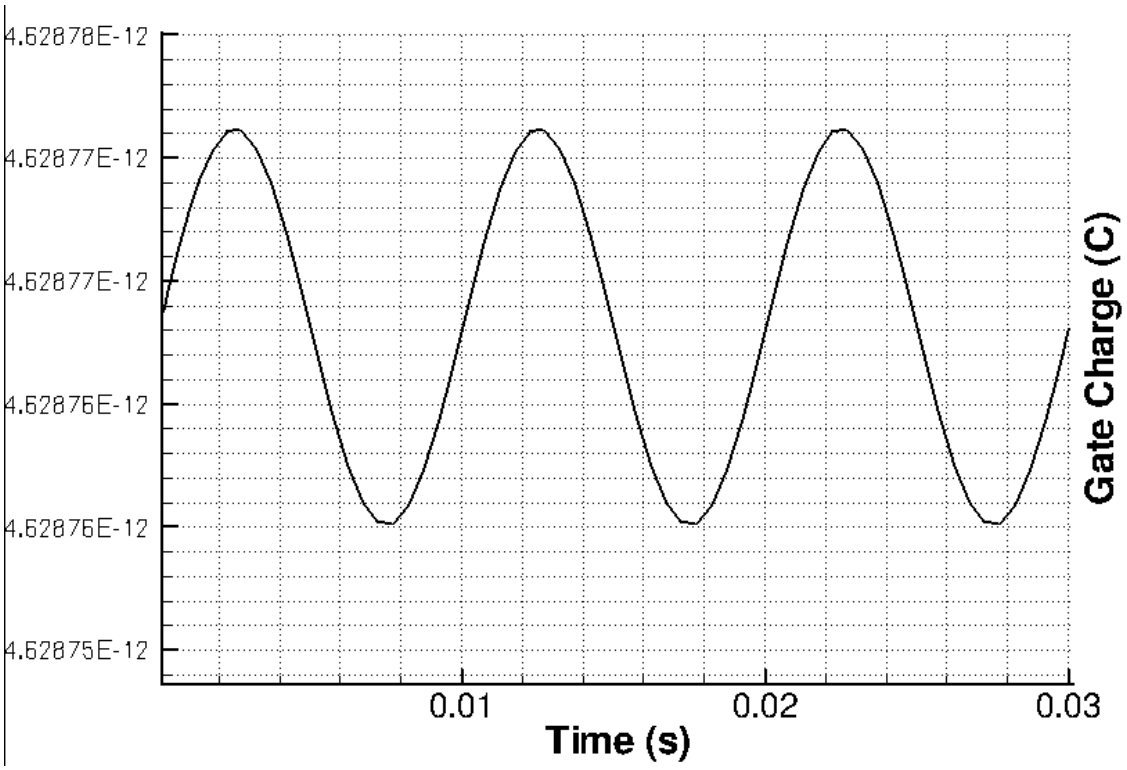

Figure 3.2.3 Gate charge varying sinusoidally with a frequency of 100 Hz and amplitude of 1.6e-17 C.

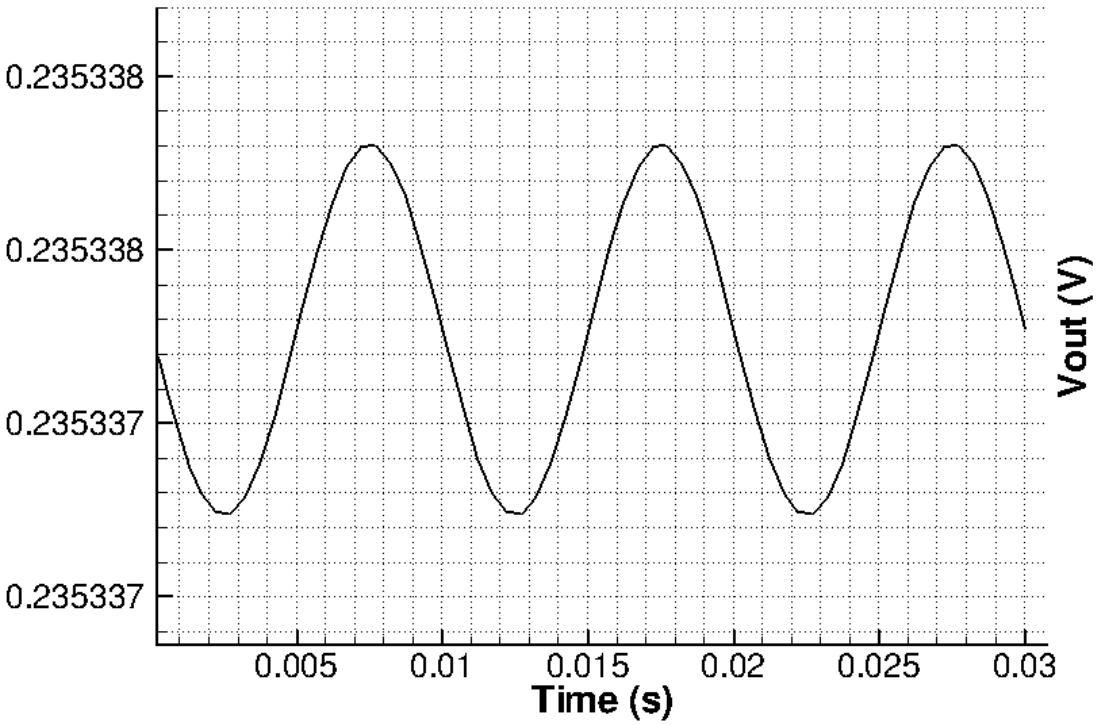

Figure 3.2.4 Output drain voltage of the common source configuration changes with the varying gate charge. The frequency of the sine function V_{out} is 100 Hz and the amplitude of the small signal voltage is 1.1e-6 V.

In reality, the device used to capture the output which is a Stanford Research 830 Lock-in Amplifier cannot read signal less than 1 μV in amplitude. Due to this limitation, the minimum ac magnetic signal detectable is 3 nT

Chapter 4

CONCLUSIONS

4.1 Analysis of the Overall Performance of the MERGT

In general, the resonant gate combined with the n-channel field effect transistor managed to amplify tiny magnetic signals. The conversion of the small ac magnetic signal to cantilever deflection then to a variation in total stored charge in the gate region of the field-effect-transistor is a great way to detect small signals since the transistor technologies has been developed to detect smaller and smaller signal over the past decades. In this thesis, oscillation of the cantilever resonant gate was first studied using COMSOL Multiphysics assuming an input magnetic signal with ac amplitude of 0.38 Oe (the value at which experimental measurement of the gate oscillation is collected) and then compared with the experimental data. Then based on considerations of flux concentration effect and cantilever stiffness variation, a new dimension for the three-layer cantilever was proposed. The new design was then verified using again COMSOL Multiphysics. After studying the mechanical properties of the resonant gate, the analysis of the electrical properties of the sensing n-channel field-effect-transistor was conducted. By building a 2D model with Sentaurus Structure Editor and simulating the device using Sentaurus Device, it has been shown that a variation of 1.6 e-17 C in gate charge will result in a variation in output voltage of 1.1 e-6 V (the minimum detectable variation in voltage with the current device is 1e-6 V).

4.2 Improvement of the Newly Designed Gate

To compare the performance of the two gates, I assumed an input ac magnetic signal of 0.38 Oe for both structures. According to [9], by increasing the cantilever aspect ratio (length/witdth) from 3 to 5, the magnetostrictive coefficient will increase by x1.5. This means that the equivalent force applied to the newly designed cantilever gate is now $(1.57\,N/m^2)\times 1.5$ which is $2.355\,N/m^2$. With these two applied forces, the COMSOL simulation returned gate deflections of 8.28 pm and 23.3 pm for the original gate and thenewly designed gate respectively. The plot below shows COMSOL Multiphysics simulation result with and applied load of $2.355\,N/m^2$

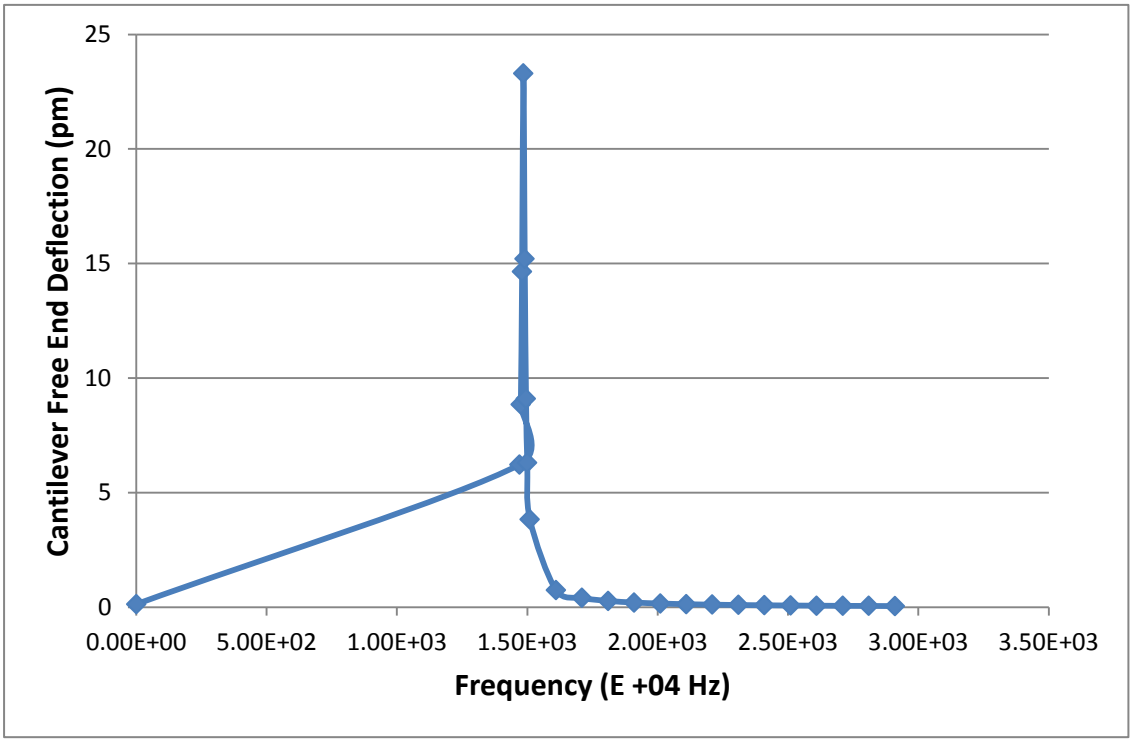

Figure 4.2.1 Frequency response of the newly designed cantilever structure under air damping with loss factor = 0.01. The load applied to the structure is $2.355\,N/m^2$. The fundamental mode of resonance of the device is at 1.285e7 Hz with amplitude of 23.3 pm.

Converting these gate deflections to variation in air-gap capacitance using the analytical modal mentioned in Chapter 3, I got 3.5235e-017 F and 1.2817e-016 F. The fact that the newly designed gate returns a larger air-gap than the original gate does indicates that the redesign indeed can improve the device sensitivity.

4.3 Future Improvement

Besides modifying the cantilever gate dimensions, there is much more space to improve the overall sensitivity of this MERGT. Considering one of the limitations imposed on the cantilever's performance by fabrication processes, which is the residual stress, if we were able to match the residual stresses in the Metglas and the Titanium layer, the initial bending of the cantilever will be largely reduced. This will turn out to be able to result in a large increase in the differential air-gap capacitance and finally an increase in the output voltage. The sensitivity improvement through this will be much more significant than by trying to optimize the cantilever gate dimensions.

Another possible improvement is through improving the signal to noise ratio (SNR) of the field-effect-transistor used. Since now, the limitation on the minimum detectable output signal is due to the noise level in the sensing field-effect-transistor, by improving the SNR, even with the same cantilever gate dimension, magnetic signal smaller than 3 nT will be detectable.

Appendix A

Study of the Impact of Thickness Ratios on the Cantilever Deflection

MATLAB m-File

```
% Subject: Titanium-Metglas-Platinum Three layer cantilever gate structure
%         Optimize thickness ratios of the three layers
% Name:    Yufei Wu
% Date:    February 15, 2012

% Titanium layer ---> layer 1
% Metglas  layer ---> layer 2
% Platinum layer ---> layer 3

clear
clc
clf
set(0,'DefaultFigureWindowStyle','docked')
%--------------------------------------------------------------------
% Define material properties
E1 = 1.16e11;               % Young's modulus for titanium in Pa
E2 = 1.7e11;                % Young's modulus for metglas in Pa
E3 = 1.68e11;               % Young's modulus for platinum in Pa
v1 = 0.32;                  % Poisson's ratio for titanium
v2 = 0.3;                   % Poisson's ratio for metglas
v3 = 0.38;                  % Poisson's ratio for platinum
r = E2/E1;
q = 1;
sigma1 = 100e9;             % Initial stress of layer 1 in Pa
sigma2 = 200e9;             % Initial stress of layer 2 in Pa
epsilon1 = sigma1/E1;       % Initial strain of layer 1
epsilon2 = sigma2/E2;       % Initial strain of layer 2
epsilon = epsilon2 - epsilon1; % Relative strain
%--------------------------------------------------------------------
lamda = 20e-6;              % Saturation magnetostrictive strain in x direction
%--------------------------------------------------------------------
w = 100e-6;                 % Cantilever width in m
l = 300e-6;                 % Cantilever length in m
t2 = 100e-9;                % Metglas layer thickness in m
%--------------------------------------------------------------------
Q1 = E1 / (1-v1^2);          % x direction stiffness for layer 1
Q2 = E2 / (1-v2^2);          % x direction stiffness for layer 2
```

```
Q3 = E3 / (1-v3^2);          % x direction stiffness for layer 3
%-------------------------------------------------------------------
n = 1;
m = 1;
cmap = hsv(10);
%-------------------------------------------------------------------
for x = 0.1:0.1:1            % t3/t2
    t3(m) = t2*x;

    for y = 1:0.1:8          % t1/t2
        t1(m,n) = t2*y;
        z0(m,n) = -0.5*(t1(m,n) + t2 + t3(m));
        z1(m,n) = 0.5*(t1(m,n) - t2 - t3(m));
        z2(m,n) = 0.5*(t1(m,n) + t2 - t3(m));
        z3(m,n) = 0.5*(t1(m,n) + t2 + t3(m));

        A(m,n) = Q1*t1(m,n)+Q2*t2+Q3*t3(m);
        B(m,n) = 0.5*(Q1*(z1(m,n)^2-z0(m,n)^2) + Q2*(z2(m,n)^2-z1(m,n)^2)...
                + Q3*(z3(m,n)^2-z2(m,n)^2));
        D(m,n) = 1/3 *( Q1*(z1(m,n)^3-z0(m,n)^3)+ Q2*(z2(m,n)^3-z1(m,n)^3)...
                + Q3*(z3(m,n)^3-z2(m,n)^3));

        Nm(m,n) = Q2*lamda*t2;
        Mm(m,n) = 0.5*Q2*(z2(m,n)^2 - z1(m,n)^2)*lamda;

        kappa(m,n) = 1./(A(m,n).*D(m,n) - B(m,n).^2) .* (-B(m,n).*Nm(m,n)...
                    +A(m,n).*Mm(m,n));
        d(m ,n) = -kappa(m,n).*l.^2/2;

        figure (1)
        plot(y,d(m,n),'o','color',cmap(m,:))
        hold on
        %-------------------------------------------------------------
        p(m,n) = t2./t1(m,n);
        t(m,n) = t2 + t1(m,n);
        rho(m,n) = t(m,n)./(2*epsilon) .* (1+ (1+p(m,n)*q*r)./(3*(1+p(m,n)).^2)...
                  .*(p(m,n).^2 + 1./(p(m,n)*q*r)));
        delta(m,n) = rho(m,n) - (rho(m,n).^2 - l^2).^0.5;
% Residual stress induced bending
        n = n+1;
    end
    m = m+1;
end
```

```
xlabel('t_titanium / t_metglas')
ylabel('Deflection (m)')
title('Gate displacement vs. Thickness ratios among Ti, Metglas, Pt')
figure (2)

tem=zeros(10,71);
dev=tem;
tem1=zeros(10,71);

for i=1:10
    tem(i,:)=d(i,(1+71*(i-1)):(71*i));
    tem1(i,:)=delta(i,(1+71*(i-1)):(71*i));
end

y=[1,1:0.1:7.9];

for i=1:70
    dev(:,i)=(tem(:,i+1)*10e5-tem(:,i)*10e5);
end

for i=1:10
    plot(y,dev(i,:),'color',cmap(i,:))
    hold on
end

xlabel('t_titanium / t_metglas')
ylabel('Rate of Change of Deflection')
title('Rate of Change of Gate displacement vs. Thickness ratios among Ti, Metglas, Pt')

figure (3)
for i=1:10
    plot(y,tem1(i,:),'color',cmap(i,:))
    hold on
end

%Differential capacitan calculation
d1 = 300e-9;                    % Distance between top resonant gate end and transistor gate
d2 = d1 + tem1;                 % Distance between top resonant gate tip and transistor gate
d_t = 0.5*(d1 + d2);

e0 = 8.85e-12;                      % Free space permittivity
A = l*w;                            % Area of gate capacitor
c0 = e0*A ./ (d2 - d1).*log(d2./d1);
```

```
del_c = c0.*tem./d_t;
del_c_T = transpose(del_c);
xlswrite('del_c_T', del_c_T)
```

Appendix B

Study of the Impact of Aspect Ratios on the Cantilever Deflection

MATLAB m-File

```
% Subject: Titanium-Metglas-Platinum Three layer cantilever gate structure
%          Optimize aspect ratio of the cantilever
% Name:    Yufei Wu
% Date:    February 15, 2012

% Titanium layer ---> layer 1
% Metglas  layer ---> layer 2
% Platinum layer ---> layer 3

clear
clc
clf
set(0,'DefaultFigureWindowStyle','docked')
%--------------------------------------------------------------------------
% Define material properties
E1 = 1.16e11;               % Young's modulus for titanium in Pa
E2 = 1.7e11;                % Young's modulus for metglas in Pa
E3 = 1.68e11;               % Young's modulus for platinum in Pa
v1 = 0.32;                 % Poisson's ratio for titanium
v2 = 0.3;                  % Poisson's ratio for metglas
v3 = 0.38;                 % Poisson's ratio for platinum
r = E2/E1;
q = 1;
sigma1 = 100e9;             % Initial stress of layer 1 in Pa
sigma2 = 200e9;             % Initial stress of layer 2 in Pa
epsilon1 = sigma1/E1;       % Initial strain of layer 1
epsilon2 = sigma2/E2;       % Initial strain of layer 2
epsilon = epsilon2 - epsilon1; % Relative strain
%--------------------------------------------------------------------------
lamda = 20e-6;              % Saturation magnetostrictive strain in x direction
t1 = 400e-9;                % Titanium layer thickness in m
t2 = 100e-9;                % Metglas layer thickness in m
t3 = 30e-9;                 % Platinum layer thickness in m
w = 100e-6;                 % Cantilever width in m
%--------------------------------------------------------------------------
Q1 = E1 / (1-v1^2);          % x direction stiffness for layer 1
Q2 = E2 / (1-v2^2);          % x direction stiffness for layer 2
```

```
Q3 = E3 / (1-v3^2);          % x direction stiffness for layer 3
%-------------------------------------------------------------------------
z0 = -0.5*(t1 + t2 + t3);
z1 = 0.5*(t1 - t2 - t3);
z2 = 0.5*(t1 + t2 - t3);
z3 = 0.5*(t1 + t2 + t3);

A = Q1*t1+Q2*t2+Q3*t3;
B = 0.5*(Q1*(z1^2-z0^2) + Q2*(z2^2-z1^2)+ Q3*(z3^2-z2^2));
D = 1/3 *( Q1*(z1^3-z0^3)+ Q2*(z2^3-z1^3)+ Q3*(z3^3-z2^3));
Nm = Q2*lamda*t2;
Mm = 0.5*Q2*(z2^2 - z1^2)*lamda;
kappa = 1/(A*D - B^2) * (-B*Nm + A*Mm);
%-------------------------------------------------------------------------
 p = t2/t1;
 t = t2 + t1;
 rho = t/(2*epsilon) * (1+ (1+p*q*r)/(3*(1+p)^2)*(p^2 + 1/(p*q*r)));
%-------------------------------------------------------------------------
for aspect = 1:1:10;
   l(aspect) = aspect*w;
   d(aspect) = -kappa*l(aspect)^2 / 2;
   delta(aspect) = rho - (rho^2 - l(aspect)^2)^0.5;
end

d1 = 300e-9;                 % Distance between top resonant gate end and transistor gate
d2 = d1 + delta;             % Distance between top resonant gate tip and transistor gate
d_t = 0.5*(d1 + d2);

e0 = 8.85e-12;                      % Free space permittivity
A = l*w;                            % Area of gate capacitor
c0 = e0*A ./ (d2 - d1).*log(d2./d1);

del_c = c0.*d./d_t;
del_c_T = transpose(del_c);
xlswrite('del_c_T', del_c_T)

x = 1:1:10;
plot(x, del_c)
xlabel('Aspect Ratio')
ylabel('Differential Capacitance')
title('Differential Capacitance vs. Aspect Ratio')
```

Appendix C

Analytical Calculation of Channel Charge Based On the Input Magnetic Signal Magnitude

```
% Conversion of gate deflection to differential charge stored on transistor
%  gate
% Date: March 27, 2012
% Name: Yufei Wu

l = 300e-6;                % Cantilever length (m)
w = 100e-6;                % Cantilever width (m)
tm = 300e-9;               % Metglas layer thickness (m)
tp = 100e-9;               % Titanium layer thickness (m)
Em = 116e9;                % Young's modulus of Metglas (Pa)
Ep = 110e9;                % Young's modulus of Titanium (Pa)
d31 = 3.4e-6;              % Magnetostrictive coefficient (1/Oe)
Hac = 3e-5;                % AC magnetic signal to be detected (Oe)
d2 = 5e-6;                 % Distance between cantilever tip and the
                           %  gate pad (m)
d1 = 500e-9;               % Distance between cantilever fixed end and
                           %  the gate pad (m)
Vgs = 3;                   % Applied gate voltage (V)
e0 = 8.84e-12;             % Permittivity of air (F/m)

A = Ep/Em;
B = tp/tm;
D = A^2*B^4 + 2*A*(2*B + 3*B^2 + 2*B^3) + 1;
Ag = l*w;
C0 = e0*Ag/(d2-d1) * log(d2/d1);
d = 0.5*(d1+d2);

defl = (3*l^2/tm) * A*B*(B+1)/D * d31*Hac
del_C = C0*defl/d

del_Q = del_C*Vgs
```

Appendix D

Sentaurus Device Command File for Id-Vg Characteristic Simulation

```
File{
    Grid          = "meshnew_msh.tdr"

    Plot          = "plot.tdr"
    Current       = "current.plt"
    Output        = "output.log"
}

Electrode{
    { Name="source"       Voltage=0.0 }
    { Name="drain"        Voltage=0.0 }
    { Name="gate"         Voltage=0.0 Barrier =-0.5}
    { Name="substrate" Voltage=0.0 }
}


Physics{
    ArearFactor = 100
    eQCvanDort
    EffectiveIntrinsicDensity( OldSlotboom )
    Mobility(
        DopingDep
        eHighFieldsaturation( GradQuasiFermi )
        hHighFieldsaturation( GradQuasiFermi )
        Enormal
    )
    Recombination(
        SRH( DopingDep )
    )
}

Plot{
*--Density and Currents, etc
    eDensity hDensity
    TotalCurrent/Vector eCurrent/Vector hCurrent/Vector
    eMobility hMobility
    eVelocity hVelocity
    eQuasiFermi hQuasiFermi
```

```
*--Temperature
    eTemperature Temperature * hTemperature

*--Fields and charges
    ElectricField/Vector Potential SpaceCharge

*--Doping Profiles
    Doping DonorConcentration AcceptorConcentration

*--Generation/Recombination
    SRH Band2Band * Auger
    AvalancheGeneration eAvalancheGeneration hAvalancheGeneration

*--Driving forces
    eGradQuasiFermi/Vector hGradQuasiFermi/Vector
    eEparallel hEparallel eENormal hENormal

*--Band structure/Composition
    BandGap
    BandGapNarrowing
    Affinity
    ConductionBand ValenceBand
    eQuantumPotential
}

Math {
    Extrapolate
    Iterations=20
    Notdamped =100
    RelErrControl
    ErRef(Electron)=1.e10
    ErRef(Hole)=1.e10
}

Solve {
    *- Build-up of initial solution:
    NewCurrentFile="init"
    Coupled(Iterations=100){ Poisson }
    Coupled{ Poisson Electron Hole}

    *- Bias drain to target bias
    Quasistationary(
        InitialStep=0.01 Increment=1.35
        MinStep=1e-5 MaxStep=0.2
```

```
    Goal{ Name="drain" Voltage= 0.05    }
){ Coupled{ Poisson Electron Hole} }

*-   gate voltage sweep
NewCurrentFile=""

Quasistationary(
    InitialStep=1e-3 Increment=1.35
    MinStep=1e-5 MaxStep=1.1
    Goal{ Name="gate" Voltage= 5 }
){ Coupled{ Poisson Electron Hole}
    CurrentPlot(Time=(Range=(0 1) Intervals=20))
}
```

Appendix E

Sentaurus Device Command File for Small Signal Analysis

```
Device NMOS1 {
    Electrode {
        { Name="source"          Voltage=0.0    }
        { Name="drain"           Voltage=0.0    }
        { Name="gate"            Voltage=0.0    Barrier=-0.55 }
        { Name="substrate" Voltage=0.0    }
    }
    File {
        Grid          = "mesh_msh.tdr"
        Plot          = "ACamplify1"
        Current = "ACamplify1"
        }
    Physics {
        AreaFactor = 100
        Mobility( DopingDependence HighFieldSaturation Enormal )
        EffectiveIntrinsicDensity(BandGapNarrowing (OldSlotboom))
    }
}
Device NMOS2{
    Electrode {
        { Name="source"          Voltage=0.0    }
        { Name="drain"           Voltage=0.0    }
        { Name="gate"            Voltage=0.0    Barrier=-0.55 }
        { Name="substrate" Voltage=0.0    }
    }
    File {Grid = "mesh_msh.tdr"
        Plot          = "MERGTcommonSource"
        Current = "MERGTcommonSource"
    }
    Physics {
        AreaFactor = 10
        Mobility( DopingDependence HighFieldSaturation Enormal )
        EffectiveIntrinsicDensity(BandGapNarrowing (OldSlotboom))
    }
}
    System {
        Vsource_pset v0 (n1 n0) { sine=(3 1e-4 100 0 0) }
        NMOS1 nmos1( "source"=n0 "drain"=n3 "gate"=n1 "substrate"=n0 )
        NMOS2 nmos2( "source"=n3 "drain"=n2 "gate"=n2 "substrate"=n0 )
        Capacitor_pset c1 ( n3 n0 ){ capacitance = 3e-14 }
```

```
    Set (n0 = 0)
    Set (n2 = 0)
    Set (n3 = 0)
    Plot "MERGTcommonSource.plt" (time() n0 n1 n2 n3 )
}
File {
    Current= "MERGT"
    Output = "MERGT"
}
Plot {
    eDensity hDensity eCurrent hCurrent
    ElectricField eEnormal hEnormal
    eQuasiFermi hQuasiFermi
    Potential Doping SpaceCharge
    DonorConcentration AcceptorConcentration
}
Math {
    Extrapolate
    RelErrControl
    Digits=5
    Notdamped=50
    Iterations=15
    NoCheckTransientError
}
Solve {
    #-build up initial solution
    NewCurrentPrefix = "ignore_"
    Coupled { Poisson }
    Quasistationary ( InitialStep=0.1 MaxStep=0.1
                                    Goal { Node="n2" Voltage=5 }
                                    Goal { Node="n3" Voltage=5 }
                                )
                                    { Coupled { Poisson Electron Hole } }
    NewCurrentPrefix = ""
    Unset (n3)
    Transient (
        InitialTime=0 FinalTime=0.03
        InitialStep=1e-5 MaxStep=5e-4 MinStep=0.5e-9
        Increment=1.3
    )
        { Coupled { nmos1.poisson nmos1.electron nmos1.contact
                        nmos2.poisson nmos2.electron nmos2.contact circuit }
        }
 }
```

Bibliography

[1] Judy, J. W. Microelectromechanical Systems (MEMS): fabrication, design and applications. Smart materials and structures. 2001; 10: 1115-1134.

[2] Liu, C. Foundations of MEMS. Upper Saddle River, N.J.: Pearson, Prentice Hall; 2006. 8 p. 17-18p. 33p.

[3] Johnson, R. C. There's more to MEMS than meets the iPhone. [Internet]. 2007 [cited 2012 January 30]; Available from:

http://eetimes.com/electronics-products/fpga-pld-products/4097066/There-s-more-to-MEMS-than-meets-the-iPhone

[4] Fujita, H. A decade of MEMS and its future. Micro Electro Mechanical Systems. 1997; 1-7.

[5] Bogue, R. MEMS sensors: past, present, and future. Sensor Review. 2007; 7-13.

[6] Harley, J. A. and Kenny, T. W. 1/F Noise Considerations for the Design and Process Optimization of Piezoresistive Cantilevers. Journal of Microelectromechanical Systems. 2000; Vol. 9, No.2.

[7] Petersen, K.E. Silicon as a Mechanical Material. Proceedings of the IEEE, 1982. 70(5): p. 420-457.

[8] COMSOL MULTIPHYSICS® User's Guide. Version 3.5a. Available from:

http://math.nju.edu.cn/help/mathhpc/doc/comsol/guide.pdf

[9] Fang, Z. et al. Enhancing the magnetoelectric response of Metglas/polyvinylidene fluoride laminates by exploiting the flux concentration effect. Applied physics letter. 2009; 95(11): 1115-1134.

[10] Wetherhold, R.C. and Chopra, H.D. Beam model for calculating magnetostriction strains in thin film and multilayers. Applied physics letter. 2001; 79 (23).

[11] Lee, K. B. Principles of Microelectromechanical Systems. IEEE Press, NJ.: A JOHN WILEY & SONS, INC; 2010. 8 p.452.

[12] Li, F. et al. Magnetoelectric Resonant Gate Transistor with NanoTesla Sensitivity. MEMS, IEEE.

ACADEMIC VITA

Yufei Wu
801 C07 West Aaron Drive
State College, PA, 16803
yufeiwu828@gmail.com

Education:

Bachelor of Science Degree in Electrical Engineering, Penn State University, Spring 2012
Minor in Physics
Honors in Electrical Engineering
Thesis Title: Simulating the Mechanical and Electrical Properties of a Designed Magnetoelectric Resonant Gate Transistor
Thesis Supervisor: Suman Datta

Awards:

Clifford B. Holt, Jr. Memorial Scholarship
Evan Pugh Award
President's Sparks Award
President's Freshman Award
Dean's List